Silicic acid leakage from the Southern Ocean: A possible explanation for glacial atmospheric pCO_2

Katsumi Matsumoto and Jorge L. Sarmiento
Atmospheric and Oceanic Sciences Program, Princeton University, Princeton, New Jersey, USA

Mark A. Brzezinski
Department of Ecology Evolution and Marine Biology and the Marine Science Institute, University of California at Santa Barbara, Santa Barbara, California, USA

Received 21 May 2001; revised 11 March 2002; accepted 12 March 2002; published 4 July 2002.

[1] Using a simple box model, we investigate the effects of a reduced Si:N uptake ratio by Antarctic phytoplankton on the marine silica cycle and atmospheric pCO_2. Recent incubation experiments demonstrate such a phenomenon in diatoms when iron is added [*Hutchins and Bruland*, 1998; *Takeda*, 1998; *Franck et al.*, 2000]. The Southern Ocean may have supported diatoms with reduced Si:N uptake ratios compared to today during the dustier glacial times [*Petit et al.*, 1999]. A similar reduction in the uptake ratio may be realized with an increased production of nondiatom phytoplankton such as *Phaeocystis*. Our model shows that reduced Si:N export ratios in the Southern Ocean create excess silicic acid, which may then be leaked out to lower latitudes. Any significant consumption of the excess silicic acid by diatoms that leads to an enhancement in their growth at the expense of coccolithophorids diminishes $CaCO_3$ production and therefore diminishes the carbonate pump. In our box model the combination of a reduced carbonate pump and an open system carbonate compensation draw down steady state atmospheric CO_2 from the interglacial 277 to 230–242 ppm, depending on where the excess silicic acid is consumed. By comparison, the atmospheric pCO_2 sensitivity of general circulation models to carbonate pump forcing is ~3.5–fold greater, which, combined with carbonate compensation, can account for peak glacial atmospheric pCO_2. We discuss the importance of the initial rain ratio of $CaCO_3$ to organic carbon on atmospheric pCO_2 and relevant sedimentary records that support and constrain this "silicic acid leakage" scenario. *INDEX TERMS:* 4805 Oceanography: Biological and Chemical: Biogeochemical cycles (1615); 4806 Oceanography: Biological and Chemical: Carbon cycling; 4255 Oceanography: General: Numerical modeling; 4267 Oceanography: General: Paleoceanography; *KEYWORDS:* glacial atmospheric pCO_2, ocean carbon cycle, box model, GCM, marine silicate cycle, Last Glacial Maximum

1. Introduction

[2] Bubbles of ancient air trapped in Antarctic ice show that the atmospheric CO_2 concentration (pCO_2) was 180–200 ppm during peak glacial times, including the Last Glacial Maximum (LGM) ~20,000 years ago. This is 80–100 ppm lower than the preanthropogenic interglacial value [*Barnola et al.*, 1987; *Petit et al.*, 1999]. The remarkable temporal correlation between records of atmospheric pCO_2, deep ocean temperatures, and continental ice volume strongly suggests that atmospheric CO_2 played a prominent role in past global climate changes [*Shackleton*, 2000]. Despite the seemingly clear importance of atmospheric CO_2 in the past climate variability, there is as yet no broadly accepted explanation for the 80–100 ppm amplitude, although a number of hypotheses have been proposed (see recent reviews by *Sigman and Boyle* [2000] and *Archer et al.* [2000a]). All previous explanations call for changes in the ocean carbon cycle, because the atmosphere is linked tightly to the ocean. More importantly, the ocean carbon reservoir is the only one that is sufficiently large and "reactive" to account for the magnitude and frequency of the recorded glacial/interglacial CO_2 cycles [*Broecker*, 1982].

[3] One of the glacial pCO_2 explanations calls for a change in the rain ratio of $CaCO_3$ to organic carbon (C_{org}) from the surface mixed layer. Each mole of sinking $CaCO_3$ particle removed from the surface carries with it 1 mol of carbon and two equivalent moles of alkalinity. Each mole of sinking flux of organic carbon removes from the surface 1 mol of total dissolved inorganic CO_2 (ΣCO_2) and at the same time adds a fraction of alkalinity that is associated with nitrogen accompanying organic carbon. All else being equal, the rain ratio of $CaCO_3$:C_{org} therefore determines the relative concentrations of alkalinity and ΣCO_2 in the surface

0886-6236/02/2001GB001442$12.00

ocean. Because pCO_2 correlates positively with ΣCO_2 but negatively with alkalinity, the rain ratio of $CaCO_3$:C_{org} has a strong impact on the atmospheric pCO_2.

[4] As part of their review of the glacial atmospheric pCO_2, *Archer et al.* [2000a] simulate the effect of reducing the $CaCO_3$:C_{org} rain ratio on atmospheric pCO_2 in their biogeochemistry model coupled to the Hamburg general circulation model (GCM) [*Maier-Reimer and Bacastow*, 1990; *Maier-Reimer*, 1993]. They reduce the rain ratio by doubling the whole ocean silica inventory and assume that the increased inventory will boost low-latitude diatom production at the expense of other phytoplankton. Today, the silicic acid to nitrate molar ratio of waters supplying the surface ocean is less than unity in large parts of the upper ocean [*Dugdale et al.*, 2001; J.L. Sarmiento et al., Global patterns of marine silicate and nitrate cycling, manuscript in preparation, 2002 (hereinafter referred to as Sarmiento et al., manuscript in preparation, 2002)]. By contrast, the Si:N molar ratio in diatoms living in low latitudes is $\sim$1:1 [*Brzezinski*, 1985]. Silicic acid is therefore a scarce commodity relative to nitrate, consistent with the assumption of *Archer et al.* [2000a]. *Harrison* [2000] also notes that available biological studies suggest that additional silicic acid can shift the species composition in favor of diatoms over calcite-secreting coccolithophorids. Since the export production of diatoms transports C_{org}, but not alkalinity (except for a minor contribution from nitrate and silicic acid), the displacement of the "other" phytoplankton by diatoms effectively amounts to a reduction in the $CaCO_3$:C_{org} rain ratio.

[5] In their simulation, *Archer et al.* [2000a] achieve a reduction in the $CaCO_3$:C_{org} rain ratio from their interglacial value of 0.20 to 0.06 and a concomitant drawdown in the atmospheric CO_2 by 70 ppm (estimated from the "uncompensated" glacial model with no land carbon transfer and the +200% H_4SiO_4 model). This drawdown nearly accounts for the full glacial/interglacial atmospheric pCO_2 amplitude. However, they dismiss this mechanism as implausible, because reasonable changes in silicate cycling in their model are unable to double the whole ocean silica inventory. *Harrison* [2000] argues that the aeolian supply of silica to the ocean may have been sufficiently higher during the LGM to make the scenario still viable. *Treguer and Pondaven* [2000] further point out that the riverine supply of silica, which is an order of magnitude higher than the aeolian flux today, may have also increased during the LGM [*Froelich et al.*, 1992].

[6] In this study we examine another mechanism that can possibly increase the availability of surface silicic acid during glacial times. Silicic acid is present in great abundance in the deep ocean and in the surface waters of the Southern Ocean, where deep waters upwell. However, the upwelled silicic acid is stripped out preferentially by Antarctic diatoms that are presently limited by iron (Fe). These diatoms precipitate Si in a Si:N ratio that is much higher than the ratio of $\sim$1 of more typical diatoms not limited by Fe [*Hutchins and Bruland*, 1998; *Takeda*, 1998; *Franck et al.*, 2000; *Pondaven et al.*, 2000]. As described in section 2, the new mechanism calls for a redistribution of silicic acid induced by an increased Fe availability in the Southern Ocean [*Brzezinski et al.*, 2002]. A simple box model is used to evaluate the mechanism and its effect on atmospheric pCO_2. We also conduct an equivalent experiment with the Princeton Ocean Biogeochemical Model in order to facilitate a comparison with the GCM results of *Archer et al.* [2000a]. We discuss the implications of these and other results for our understanding of glacial atmospheric pCO_2. Finally, relevant sedimentary evidence is discussed in order to evaluate the assumptions and predictions of the proposed mechanism.

2. Silicic Acid Leakage Scenario

[7] Modern Antarctica surface waters have an approximate silicic acid concentration of 60 μmol kg^{-1} and nitrate concentration of 25 μmol kg^{-1} on an annual basis [*Levitus et al.*, 1993] (also, see recent U.S. Joint Global Ocean Flux Study (JGOFS) in situ measurements along 170°W [*Smith et al.*, 2000]). The Si:N ratio is high in these surface waters, because they are linked closely to deep waters that have Si:N $\gg$ 1 by strong vertical mixing. These surface waters support primary production with a large contribution from diatoms that incorporate 4–5 times more silica per unit organic matter than those in most other regions of the world ocean [*Pondaven et al.*, 2000; *Brzezinski et al.*, 2001; Sarmiento et al., manuscript in preparation, 2002]. As these Antarctic surface waters are advected northward by Ekman transport, the preferential uptake of silicic acid over nitrate causes the in situ Si:N ratio to drop to unity or less. This is clearly seen in the subantarctic in the Levitus data set [*Levitus et al.*, 1993] as well as in JGOFS measurements [*Smith et al.*, 2000]. This Si:N $\leq$ 1 signal then propagates northward into the warm surface waters by direct mixing of subantarctic waters and by the advection of Subantarctic Mode Water, a low-density variety of Antarctic Intermediate Water that invades the middle to lower thermocline [*McCartney*, 1977].

[8] Excess silicic acid would be expected in the glacial subantarctic and Subantarctic Mode Water if today's preferential uptake of silicic acid over nitrate were reversed. This possibility is hinted at by recent incubation experiments that demonstrate that the addition of Fe to Fe-depleted water samples lowers the Si:N uptake ratio by diatoms from $\sim$4:1 [*Franck et al.*, 2000; *Pondaven et al.*, 2000] to $\sim$1:1 [*Hutchins and Bruland*, 1998; *Takeda*, 1998; *Franck et al.*, 2000]. Also, the very high dust contents in Antarctic ice cores during glacial periods indicate that aeolian Fe delivery to the glacial Southern Ocean was very high [*Petit et al.*, 1999].

[9] A number of lines of paleoceanographic evidence are consistent with a reduced preferential uptake of silicic acid in Antarctic surface waters during the LGM. First, sedimentary opal accumulation rates normalized by ^{230}Th concentrations are lower during the LGM than during the Holocene in the glacial Antarctic sediments, south of the modern Polar Front [*Kumar et al.*, 1995; *Francois et al.*, 1997; *Chase et al.*, 2002; *Anderson et al.*, 2002]. Second, sedimentary δ^{30}Si measurements from Antarctic sediments indicate that the depletion of surface silicic acid was lower there during LGM than during the Holocene [*De La Rocha*

et al., 1998]. Third, sedimentary $\delta^{15}N$ data from Antarctic sediments suggest that nitrate utilization was higher during LGM times than during the Holocene [*Francois et al.*, 1997]. In a study closely related to this one, *Brzezinski et al.* [2002] extend sedimentary $\delta^{30}Si$ and $\delta^{15}N$ records beyond the LGM to show that the temporal variation of the two measurements is antiphased even in previous glacial periods.

[10] An integral aspect of the proposed scenario is the effect that Fe has on the overall new production. Large-scale field experiments in the eastern equatorial Pacific and the Southern Ocean [*Martin et al.*, 1994; *Coale et al.*, 1996; *Boyd et al.*, 2000] confirm incubation experiments that show that Fe addition to Fe-depleted systems significantly enhances phytoplankton nitrate uptake [*Martin and Fitzwater*, 1988]. This response combined with the lower Si:N uptake ratios of Fe-replete diatoms means that the level of nitrate depletion associated with a given amount of silicic acid use increases. Therefore the greater Fe availability in the Southern Ocean may increase new production in Antarctic waters while simultaneously causing silicic acid ''leakage'' from the glacial Southern Ocean to lower latitudes. To leave behind excess silicic acid, however, the reduced silicic acid use resulting from lower Si:N uptake ratios must not be overtaken by the increased silicic acid use by an overall enhancement in the diatom stock.

[11] In addition to the postulated reduction in silica requirement by Antarctic diatoms during glacial times, a reduced stock of diatoms would also be able to create an excess pool of silicic acid, even with the high silica requirement of the modern Antarctic diatoms. The diatom stock can be reduced by an increased production of nondiatom phytoplankton such as *Phaeocytis*, a common soft-tissue phytoplankton in Antarctic surface waters today, at the expense of diatoms. Today, *Phaeocystis* is associated with high concentrations of dimethylsulphide [*Ditullio and Smith*, 1995]. Elevated concentrations of dimethylsulphide-related sulphur compounds in the Vostok ice core during glacial times [*Legrand et al.*, 1991] suggest increased growth of *Phaeocystis* during those times [*Martin*, 1992]. The two triggering mechanisms of excess silicic acid are not exclusive and cannot be distinguished here, because *Phaeocystis* leaves no obvious sedimentary record behind, and our simple model would make identical predictions for the two mechanisms.

[12] The fate of any excess silicic acid in glacial Antarctic surface waters is not entirely clear. In this study we evaluate two possibilities. First, it may leak out from the Southern Ocean into the low-latitude surface waters and enhance the growth of diatoms at the expense of other phytoplankton, as we first envisioned. Second, excess silicic acid in Antarctic surface waters may be entirely consumed in the subantarctic surface waters just to the north (R. F. Anderson, personal communication, 2001). Unlike the Antarctic sediments, the subantarctic sediments in the Atlantic and Indian sectors to the north of the modern Polar Front show that Th^{230}-normalized sedimentary opal accumulation rates were higher during the LGM than during the Holocene [*Kumar et al.*, 1995; *Francois et al.*, 1997; *Anderson et al.*, 2002]. A very rough areal integration indicates that the overall opal burial in those two sectors was about the same during the LGM and Holocene. Assuming that Southern Ocean opal burial reflects surface opal production [*Nelson et al.*, 2002], the sedimentary evidence thus suggests that the opal production in those two sectors was about the same during the two times. On the supply side a recent hydrographic reconstruction of the glacial Southern Ocean based on foraminiferal $\delta^{18}O$ suggests that the large-scale vertical circulation was also similar during the LGM and the Holocene [*Matsumoto et al.*, 2001]. This implies that the upwelling flux of silicic acid was not significantly different. The silica budget argument would predict that with no significant change in either the supply or utilization of silicic acid in the surface Southern Ocean, there would have been no more unused silicic acid during the LGM than today. This argument allows excess Antarctic silicic acid to leak out just to the subantarctic, where it is consumed entirely with no leakage to the low-latitude surface waters. Although we separately analyze these two variations of silicic acid leakage, they are not mutually exclusive.

[13] However, there are a number of difficulties with this silica budget argument. First, the linear scaling assumed between opal burial and production may have been complicated by the dependence of water column opal dissolution on temperature [*Kamatani*, 1982; *Hurd and Birdwhitell*, 1983]. Opal preservation in the sediments was likely more efficient in the colder glacial ocean. Second and more importantly, the limited number of estimates of Th^{230}-normalized opal accumulation rates available from the Pacific sector of the Southern Ocean subantarctic are inconsistent with those from the Atlantic and Indian sectors [*Chase et al.*, 2002]. Therefore the silica budget argument may not hold for the entire Southern Ocean but only for the Atlantic and Indian sectors. Finally, the argument assumes a constant silica inventory of the ocean, which may have increased from external sources, such as aeolian supply [*Harrison*, 2000] and river input [*Froelich et al.*, 1992].

3. Model Description

[14] A box model with eight ocean boxes underlying a well-mixed atmosphere (Figure 1, Table 1), was constructed in order to simulate the Si:N $\leq$ 1 observed in the subantarctic and low-latitude surface waters. Initial attempts to simulate the observed silicic acid distributions with extant models, such as the three-box model of *Toggweiler and Sarmiento* [1985] and the seven-box model of *Toggweiler* [1999] were not successful, due primarily to their deficient spatial resolution of the Southern Ocean.

[15] The new model is based on the seven-box model of *Toggweiler* [1999] but has one extra Southern Ocean surface box, which proved critical to simulate the desired features. The extra box allows for a distinction between the polar and subantarctic surface waters and a slightly more realistic representation of how the deep ocean ventilates in the Southern Ocean (Figure 1). Upwelling in the modern Southern Ocean occurs in the vicinity of the Antarctic Divergence in the form of Circumpolar Deep Water, which is predominantly composed of the North Atlantic Deep Water (NADW) in the Atlantic sector. In the model this

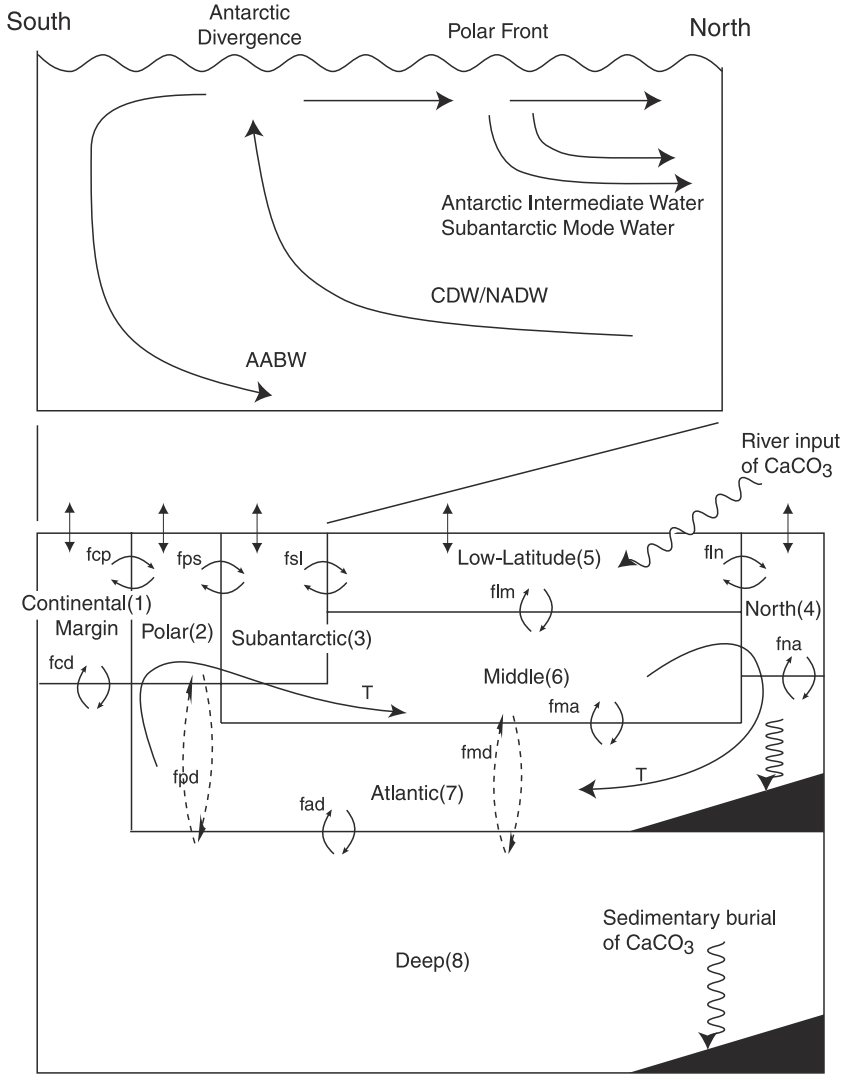

Figure 1. (top) Schematic diagram of Southern Ocean meridional circulation and (bottom) eight-box model. Box names are followed by their numerical indices. Wiggle arrows indicate a throughput of ocean alkalinity: river input into Low-Latitude surface box and sedimentary burial in Atlantic and Deep boxes. Other arrows indicate water and air-sea exchange fluxes.

Table 1. Model Dimensions and Interglacial Control Setting[a]

Ocean Boxes	Fractional Area, % (10^{12} m^2)	Box Depth, m	Volume, 10^{15} m^3	Export Production: Organic-C, Gt C yr^{-1}	Export Production: Diatom Fraction, %	Export Production: Si:N, Ratio
Continental Margin	3.0 (10.5)	250	2.62	0.47	90.0	6.0
Polar	7.0 (24.4)	250	6.11	0.53	90.0	6.0
Subantarctic	7.0 (24.4)	250	6.11	0.54	70.0	6.0
North	3.0 (10.5)	250	2.62	0.65	60.0	3.0
Low-Latitude	80.0 (279.2)	100	27.92	2.84	50.0	1.5
Middle	–	500	117.79	–	–	–
Atlantic	–	900	144.14	–	–	–
Deep	–	3700	984.71	–	–	–
Total Ocean	100.0 (349.0)	–	1292.00	5.03	–	–

[a]Most physical dimensions are from seven-box model of *Toggweiler* [1999], which was itself derived from three-box model of *Toggweiler and Sarmiento* [1985]. High-latitude surface boxes of eight-box model occupy 20% of total ocean area, compared to 15% for three-box model and 25% for seven-box model. In eight-box model the Middle box reaches 500 m, compared to 1000 m in seven-box model. Bottom of Atlantic box is set to 900 m, as opposed to 2000 m in seven-box model, so that volume of North Atlantic Deep Water is more realistic. Organic carbon production was obtained from inverse model (see text and Appendix B).

upwelling occurs in the Polar box and is represented by water fluxes *fpd*, which bring up waters from the Deep box, and the thermohaline flux *T*, which upwells NADW from the Atlantic box. The Subantarctic Mode Water forms in the Subantarctic box, whose southern boundary with the Polar box represents the Polar Front. The vertical mixing term *fcd* in the Continental Margin box accounts for the formation of Antarctic Bottom Water and the ventilation of the deep water along the Antarctic margin.

[16] The model has no separate ocean basins. Fluxes *fpd* and *fmd* allow the Deep box, representing the Indo-Pacific deep water, to communicate directly with the Polar and Middle boxes and account for the absence of NADW in the Indian and Pacific basins. The two boxes would be immediately overlying the Deep box in the absence of the Atlantic box. The mixing term *fpd* ventilates the Deep box in the Southern Ocean but is not completely analogous to Circumpolar Deep Water upwelling at the Antarctic Divergence due to coarse model resolution.

[17] The model has eight state variables: silicic acid, nitrate, oxygen, potential temperature, alkalinity, ΣCO_2, $\delta^{13}C$, and $\Delta^{14}C$. Salinity is fixed everywhere to 35 practical salinity units (psu), to which nitrate, silicic acid, alkalinity, and ΣCO_2 are normalized. Temperature, 35-psu salinity, alkalinity, and ΣCO_2 are used to compute the solubility and the disassociation constants of the carbon system and pCO_2 under the condition of chemical equilibrium [*Dickson and Goyet*, 1994]. Surface temperatures and oxygen contents are prescribed to their initial values. The gas exchange of CO_2, $^{13}CO_2$, and $^{14}CO_2$ with the atmosphere is modeled explicitly. The transfer of CO_2 is driven by the pCO_2 gradient across the air-sea interface and a "piston velocity" of 3 m day^{-1} [*Toggweiler and Sarmiento*, 1985]. The transfer of carbon isotopes is described in Appendix A.

[18] Nitrate serves as the main nutrient that accounts for organic carbon production. The nitrate concentration in the Low-Latitude surface box drives its new production by restoring the nitrate concentration to its initial value. Production and remineralization of organic matter is assumed to occur with a stoichiometry of $P:N:C_{org}:-O_2 = 1:16:117:170$ [*Anderson and Sarmiento*, 1994]. Remineralization of particulate organic matter and $CaCO_3$ follows the suggested vertical flux profiles of *Yamanaka and Tajika* [1997]. For lack of information, opal dissolution is assumed to follow the deeper remineralization profile of $CaCO_3$.

[19] *Nelson et al.* [1995] suggest that diatom contribution to primary production is roughly 35% in oligotrophic oceans and 75% in coastal zones. Here we simply assume a diatom contribution of 50% in the Low-Latitude box (Table 1), which contains both types of ocean regime. The high-latitude surface waters, particularly in the Southern Ocean, have much higher diatom contributions [*Nelson et al.*, 1995], for which we assume 90% in the two southernmost boxes (Table 1). Simulations with different diatom fractions show that when the model is tuned reasonably well to the modern nutrient distributions, the model pCO_2 reduction and silicic acid redistribution do not vary significantly in response to the proposed scenario forcing (i.e., changes in the high-latitude silicic acid utilization relative to nitrate). Rather, a more important model parameter is the Si:N export ratio. Observations indicate that Si:N uptake ratio by diatoms is ~4:1 in Fe-deficient high-latitude surface waters [*Franck et al.*, 2000; *Pondaven et al.*, 2000] and is 1:1 in Fe-replete low-latitude surface waters [*Hutchins and Bruland*, 1998; *Takeda*, 1998]. However, the export ratio should be higher than the uptake ratio, because organic matter degrades much more readily than opaline frustules of diatoms. We expect the differential remineralization to be accentuated in high-latitude surface boxes that are thicker and colder than in the Low-Latitude surface box. We therefore assume a Si:N export ratio of 6 in the Southern Ocean surface boxes and 1.5 in Low-Latitude box (Table 1). The exact ratios do not significantly affect the main results of this study, as long as the high-latitude surface boxes have higher ratios than the Low-Latitude box as indicated by observations.

[20] As we will show below, a model parameter that is key to atmospheric pCO_2 is the modern export rain ratio of $CaCO_3:C_{org}$. Here we assume a global average of 0.1 in contrast to previously assumed values of 0.2–0.3 [*Toggweiler and Sarmiento*, 1985; *Broecker and Peng*, 1987; *Sigman et al.*, 1998; *Toggweiler*, 1999; *Archer et al.*, 2000a]. The observational basis for 0.2–0.3 comes from *Li et al.* [1969], who used late 1960s in situ CO_2 measurements to calculate excess alkalinity and ΣCO_2 in the Atlantic and Pacific deep waters. The difference between average deep and surface alkalinity and ΣCO_2 concentrations was simply attributed to remineralization of exported particulates. Also, the method of *Li et al.* [1969] does not account for the nitrate contribution to alkalinity.

[21] We offer two reasons to suggest that the ratio of 0.1 is more appropriate. First, the excess alkalinity and ΣCO_2 in the deep waters relative to the surface waters are affected by the preferential remineralization of organic matter over calcite, a factor apparently neglected by *Li et al.* [1969]. When this is taken into consideration, *Yamanaka and Tajika* [1997] predict that the $CaCO_3:C_{org}$ rain ratio should be 0.12 or less. Furthermore, they offer a detailed analysis of $CaCO_3$ cycling with a GCM and suggest that the modern ratio is 0.08–0.10. Second, we have recently applied a transport divergence approach to the 1990s measurements obtained as part of World Circulation Experiment and to the 1980s data from the Atlantic surveys (Transient Tracers in the Ocean and South Atlantic Ventilation Experiment) in order to estimate the modern rain ratio of $CaCO_3:C_{org}$ (J. L. Sarmiento et al., A new estimate of the $CaCO_3$:organic carbon export ratio, submitted to *Global Biogeochemical Cycles*, 2002). In essence, this method estimates the supply ratio of alkalinity and ΣCO_2 to the surface mixed layer from their concentration gradients across the base of the mixed layer. A steady state assumption with regard to their mixed layer concentrations then requires that the export ratio match the supply ratio. Their preliminary analysis indicates that the rain ratios in all three ocean basins are more consistent with the lower value of 0.1 [*Yamanaka and Tajika*, 1997] than with the traditional values of 0.2–0.3.

[22] The most important parameters in ocean carbon cycle models are arguably those that relate to circulation and surface production. Here we obtained them objectively in an inverse model (Appendix B). Even in simple box

Table 2. Preindustrial State Corresponding to Eight-Box Model[a]

Boxes	Θ, °C	NO_3^-, μmol kg^{-1}	H_4SiO_4, μmol kg^{-1}	O_2, μmol kg^{-1}	Alkalinity, μmol eq kg^{-1}	ΣCO_2, μmol kg^{-1}	$\delta^{13}C$, ‰	$\Delta^{14}C$, ‰
Ocean								
Continental Margin	−1.0 ± 0.4	26.9 ± 4.0	60.0±13.3	295 ± 22	2412 ± 58	2246 ± 67	1.0± 0.5	−140 ± 30
Polar	2.5 ± 2.4	22.4 ± 4.6	34.8 ± 13.3	294 ± 22	2388 ± 58	2211 ± 67	1.0 ± 0.5	−120 ± 30
Subantarctic	6.0 ± 2.4	17.8 ± 4.6	9.4 ± 6.2	293 ± 17	2351 ± 58	2115 ± 67	1.5 ± 0.5	−80 ± 30
North	3.3 ± 2.3	8.7 ± 2.2	5.8 ± 1.3	313 ± 19	2325 ± 38	2097 ± 51	1.5 ± 0.5	−55 ± 30
Low-Latitude	22.1 ± 5.4	3.1 ± 4.0	4.7 ± 4.4	208 ± 37	2322 ± 58	1954 ± 67	2.0 ± 0.5	−40 ± 30
Middle	12.3 ± 2.4	17.6 ± 7.6	17.5 ± 12.2	138 ± 69	2322 ± 33	2120 ± 56	1.6 ± 0.5	−70 ± 30
Atlantic	3.2 ± 1.2	21.3 ± 3.9	31.6 ± 14.0	238 ± 23	2340 ± 25	2177 ± 13	0.9 ± 0.5	−100 ± 30
Deep	1.8 ± 0.8	34.1 ± 4.2	102.9 ± 27.9	153 ± 44	2435 ± 24	2329 ± 39	0.2 ± 0.5	−177 ± 30
Atmosphere						280 (ppm)	−6.50	0.00

[a] Preindustrial atmospheric pCO_2 and $\delta^{13}C$ determined from Antarctic ice core measurements are ∼280 ppm and −6.5‰, respectively [*Barnola et al.*, 1987; *Leuenberger et al.*, 1992; *Petit et al.*, 1999; *Smith et al.*, 1999]. Preindustrial atmospheric $\Delta^{14}C$ by convention is defined to be 0‰ [*Stuiver*, 1980]. Atlantic box reflects Atlantic waters between 1500 and 3500 m. Deep box includes Indian and Pacific waters deeper than 1500 m and Atlantic waters deeper than 3500 m. Middle box is approximated by $\sigma_0 = 26.5$ isopycnal surface, whose average depth is ∼300 m. On this surface between 40°S and 40°N, mean silicic acid and nitrate concentrations are, respectively, 17.50 and 17.60 μmol kg^{-1}, yielding Si:N ≤ 1 [*Levitus et al.*, 1993; *Levitus and Boyer*, 1994; *Levitus et al.*, 1994]. Low-Latitude box includes waters shallower than 100 m, equatorward of 40°S and 60°N. North box represents site of North Atlantic Deep Water (NADW) formation and reflects Atlantic surface properties between 60°N and 75°N, shallower than 250 m. Subantarctic box represents surface subantarctic between Polar Front and Subtropical Front. Here we use a 2°C isotherm at 100 m to identify Polar Front [*Belkin and Gordon*, 1996]. Subtropical Front is delineated here by a 10°C isotherm at 100 m [*Orsi et al.*, 1995]. Subantarctic box is represented by mean property values on the 100-m-depth surface between 2° and 10°C isotherms. Similarly, Continental Margin box is represented by a surface at 100-m water depth poleward of the 0°C isotherm. Polar box is simply a mean of Subantarctic and Continental Margin boxes. Potential temperature, nitrate, silicic acid, and oxygen values are from Levitus data [*Levitus et al.*, 1993; *Levitus and Boyer*, 1994; *Levitus et al.*, 1994]. Alkalinity values (μmol equivalent kg^{-1}) and ΣCO_2 values are from survey data of World Ocean Circulation Experiment (WOCE) (R. M. Key, personal communication, 2001), Transient Tracers in the Ocean North Atlantic Study [*Brewer et al.*, 1986], and Geochemical Ocean Sections Study (GEOSECS) [*Bainbridge*, 1981; *Broecker et al.*, 1982; *Weiss et al.*, 1983]. Nitrate, silicic acid, alkalinity, and ΣCO_2 values are normalized to 35 practical salinity units. ΣCO_2 values are further adjusted for anthropogenic contributions (μmol kg^{-1}) [*Gruber*, 1998; *Sabine et al.*, 1999]: Continental Margin = 30; Polar = 30; Subantarctic = 40; North = 40; Low-Latitude = 40; Middle = 25; Atlantic = 10; and Deep = 5. GEOSECS ΣCO_2 are assumed to contain 30% less anthropogenic contribution than WOCE ΣCO_2 data [*Sabine et al.*, 1999]. Subsurface $\delta^{13}C$ were estimated from nitrate concentrations, stoichiometry of PO_4:NO_3 = 1:16, and a phosphate-$\delta^{13}C$ relationship of $\delta^{13}C = 2.8 - 1.1[PO_4]$ [*Lynch-Stieglitz et al.*, 1995]. Atlantic box was further modified by subtracting 0.4‰ to remove air-sea gas exchange signal of NADW [*Broecker and Maier-Reimer*, 1992]. Values for $\Delta^{14}C$ were obtained from *Broecker et al.* [1998], *Broecker and Peng* [1982], and *Toggweiler et al.* [1989]. Uncertainty represents first standard deviation of mean where calculated. A large and constant uncertainty was assigned arbitrarily to $\delta^{13}C$ and $\Delta^{14}C$ to estimate error in inversion results by Monte Carlo simulations (see Appendix B).

models the number of model parameters exceeds the number of observational constraints. Previous box model studies determined the appropriate values for such parameters by individually tuning them "by hand" to match, for example, the expected atmospheric and oceanic $\Delta^{14}C$. This process is not only subjective but becomes increasingly difficult as the numbers of variables and boxes increase. The inverse model approach is able to reduce the arbitrariness involved in manual tuning by determining model parameters objectively and simultaneously. The solutions of the inverse model minimize the mismatch between the preindustrial state of the ocean and atmosphere (Table 2) and steady state model predictions in the least squares sense.

[23] Finally, the prognostic model is coupled to a simple sediment model that simulates the accumulation and dissolution of calcite on the seafloor (Appendix C). The inclusion of sediments allows the model to be "open" with respect to the alkalinity budget. At steady state the riverine input of alkalinity from the weathering of emergent carbonates on land exactly balances the removal of alkalinity by sediment burial of $CaCO_3$. Perturbations to the ocean carbonate system can be compensated by changes in the depth of the "calcite lysocline," which marks the transition between the shallower sediments where $CaCO_3$ is preferentially preserved and the deeper sediments where most of the falling $CaCO_3$ particles dissolve. The depth of the calcite lysocline therefore mediates the distribution of $CaCO_3$ burial. A primary control of the lysocline depth is the calcite saturation depth, where bottom water carbonate ion concentration equals the carbonate ion concentration saturated with respect to calcite (see Appendix C). Calcite burial occurs predominantly above the carbonate saturation horizon, where bottom waters are supersaturated, and dissolution driven by undersaturation occurs below the saturation horizon. A shoaling of the saturation horizon decreases the area of seafloor bathed by supersaturated bottom waters and hence reduces calcite burial. A deepening of the saturation depth has the opposite effect. The response of the lysocline to perturbations in the ocean carbonate system represents a negative feedback that drives alkalinity removal by calcite burial toward a balance with riverine input of alkalinity [*Broecker and Peng*, 1982]. In studies of glacial atmospheric pCO_2 it is critical to be able to simulate the calcite lysocline, because it exerts a strong control on atmospheric pCO_2 [*Sigman et al.*, 1998; *Archer et al.*, 2000a].

4. Inverse Modeling and Interglacial Control

[24] The interglacial control represents a model steady state that best resembles the preindustrial ocean and atmosphere. We use the prognostic model using the best fit circulation and production parameters from the inverse model to predict it. To illustrate the benefit gained from inversion, two sets of steady state predictions are compared

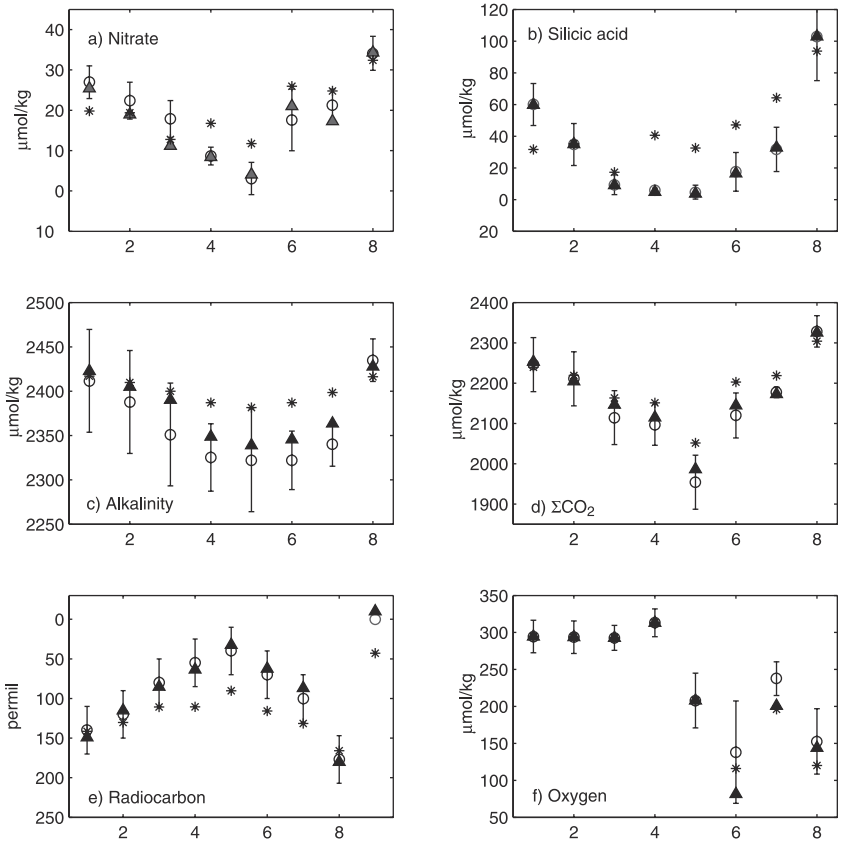

Figure 2. Observed and steady state distributions predicted by prognostic model. (a) Nitrate. (b) Silicic acid. (c) Alkalinity. (d) ΣCO_2. (e) $\Delta^{14}C$. (f) Oxygen. Ocean boxes are indicated on horizontal axis (1–8; see Figure 1). Ninth index in $\Delta^{14}C$ panel refers to atmosphere. Observed mean and standard deviations are from Table 2 (circles and bars, respectively). Asterisks indicate model results obtained using prior estimates of circulation and production parameters (i.e., no inversion). Triangles represent interglacial control obtained using an optimal set of inverse model solutions (Table B1).

in Figure 2. One set shows the state obtained using the prior estimates of the solutions or the first guess of what the parameters might be (see Table B1). When hand tuning a model, the prior estimates are essentially what one would start with. Most of the predicted values are outside the range of observed values, with conspicuously poor performance reproducing silicic acid, alkalinity, and radiocarbon distributions (asterisks in Figure 2).

[25] The prognostic model produces a superior match to the observations when it uses inverse model solutions that were moderately constrained to prior estimates (triangles, Figure 2). Most of the predicted variables are within the range of observed values (Table 3). The predicted nitrate and silicic acid concentrations are such that the desired Si:N ≤ 1 is achieved in the Low-Latitude, Subantarctic, and Middle boxes. The atmospheric pCO_2 of 277 ppm is also appropriate. A notable mismatch is the atmospheric $\Delta^{14}C$ of 9.9‰ instead of the target 0.0‰. This indicates that with regard to radiocarbon alone, the deep ocean is not ventilating enough. This sort of discrepancy is not surprising, because simplified box models that are tuned with one tracer will likely be inconsistent when the same models are tuned with a different tracer [*Siegenthaler and Joos*, 1992]. Since the inverse problem at hand is overdetermined and the inversion was constrained by multiple tracers, some mismatch is inevitable.

[26] The optimal organic carbon production obtained by the inverse model is slightly over 5 Gt C yr^{-1} (Gt = 10^{15} grams) globally (Tables 1 and B1). In comparison, the combination of satellite-derived chlorophyll concentrations and algorithms of phytoplankton carbon fixation [*Behrenfeld and Falkowski*, 1995] and observationally derived *f* ratios predicts a production of ~11 Gt C yr^{-1} [*Laws et al.*, 2000]. A number of GCMs can support roughly that amount of new production [*Yamanaka and Tajika*, 1997; *Archer et al.*, 2000a; *Gnanadesikan et al.*, 2002], although still higher levels can be supported by increasing nutrient supply to the mixed layer by enhanced vertical diffusion. However, simple box models can support only a fraction of the estimated 11 Gt C yr^{-1} [*Toggweiler and Sarmiento*, 1985; *Sigman et al.*, 1998; *Toggweiler*, 1999], because the lack of vertical spatial resolution limits their ability to correctly represent the processes that supply nutrients to the surface. The inherent limit of simple box models in this respect becomes apparent, when the eight-box model is forced to support 10 Gt C yr^{-1}. In this case the rate of

Table 3. Model State for Interglacial Control[a]

Boxes	θ, °C	NO_3^-, μmol kg^{-1}	H_4SiO_4, μmol kg^{-1}	Si:N, ratio	O_2, μmol kg^{-1}	Alkalinity, μmol-eq kg^{-1}	ΣCO_2, μmol kg^{-1}	$\delta^{13}C$, ‰	$\Delta^{14}C$, ‰
Ocean									
Continental Margin	−1.0	25.4	59.8	2.4	295	2423	2259	1.4	−149
Polar	2.5	19.0	35.0	1.8	294	2405	2204	1.7	−115
Subantarctic	6.0	11.2	9.1	0.8	293	2309	2147	2.2	−85
North	3.3	8.4	4.9	0.6	313	2349	2115	1.8	−63
Low-Latitude	22.1	4.1	3.7	0.9	208	2339	1987	2.0	−32
Middle	16.9	21.0	16.5	0.8	81	2346	2145	0.8	−62
Deep	2.3	34.3	102.9	3.0	144	2428	2326	0.5	−180
Atmosphere							277 ppm	−6.6	9.9
Inventory		4.01×10^{16}	1.11×10^{17}			3.19×10^{18}	3.07×10^{18}	3.07×10^{18}	2.60×10^{18}

[a] This prognostic model state was obtained by using inverse model solutions from Table B1. Total inventories are given in moles, $\delta^{13}C$ and $\Delta^{14}C$ inventories in pseudo-moles (see Appendix A). All inventories are consistent with those from *Toggweiler and Sarmiento* [1985] and with estimates from *Levitus et al.* [1993] data.

deep ventilation has to be so high that in addition to nutrients, very negative $\Delta^{14}C$ is brought up to the surface. This drives the atmospheric $\Delta^{14}C$ to excessively negative values.

5. Results

5.1. Silicic Acid Leakage and Atmospheric CO_2 Drawdown in Box Model

[27] The reduction in the Si:N uptake ratio of Antarctic diatoms as a result of increased Fe supply is simulated in the eight-box model by reducing the Si:N export ratio in the Southern Ocean surface boxes, keeping all other parameters at their interglacial control values. Figure 3 shows the results of allowing excess silicic acid to reach the Low-Latitude box. As the export ratio is reduced from the interglacial value of 6 to 1, silicic acid leakage from the Southern Ocean becomes clearly evident in the monotonic increase of the Low-Latitude silicic acid concentration from 3.7 to 35.3 μmol kg^{-1} (asterisks in Figure 3a). This result is relatively insensitive to the model parameters, as very similar results are obtained with the eight-box model even when it is initially tuned to the modern state with different sets of model parameters. Qualitatively similar silicic acid leakage was also simulated in the seven-box model of *Toggweiler* [1999], although its interglacial control was not able to simulate the modern silicic acid distribution nearly as well as the eight-box model.

[28] To simulate the utilization of this extra silicic acid by diatoms, the silicic acid concentration in the Low-Latitude box is restored to its initial concentration. This increases the contribution of diatoms to the new production with increasing silicic acid leakage (triangles in Figure 3b). With total export organic carbon production held constant, the diatom fraction in the Low-Latitude box reaches nearly 100% by the time the Southern Ocean Si:N export ratio is down to 1 from its interglacial value. At this point the carbonate pump is minimal, because diatoms in the Low-Latitude box have largely replaced nondiatom phytoplankton. The global $CaCO_3$:C_{org} rain ratio, however, does not reach zero (triangles in Figure 3c), because the replacement is not yet complete and the export production in high-latitude surface boxes still includes a small calcite production. When the carbonate pump is minimal, atmospheric pCO_2 is reduced by 9 ppm, from the interglacial 277 to 268 ppm (triangles in Figure 3d).

[29] The second case of the leakage scenario calls for a complete consumption of excess silicic acid by diatoms in the subantarctic, not allowing any leakage to reach the low-latitude surface waters. In this case, we find that the excess silicic acid cannot be consumed entirely in the Subantarctic box by simply increasing its diatom fraction (Figure 4), because the total organic carbon production there was much lower to begin with than in the Low-Latitude box. The diatom fraction completely saturates when the Si:N export ratio is down from 6 to just 5. Thereafter the silicic acid concentration increases and then escapes to lower latitudes. The atmospheric CO_2 drawdown in this case is merely 2 ppm. It is possible, of course, to utilize more silicic acid, if the initial diatom fraction in the Subantarctic box were lower than the prescribed 70% (Table 1). However, the atmospheric CO_2 drawdown would still be 2 ppm, because the total change in $CaCO_3$:C_{org} would remain unchanged. The reason is that the initial $CaCO_3$:C_{org} ratio of nondiatoms would have be lowered to compensate for the reduced diatom fraction so as to maintain a global $CaCO_3$:C_{org} rain ratio of 0.1.

[30] Alternatively, more excess silicic acid can be utilized if the overall production in the Subantarctic box is enhanced, another effect that is expected from increased Fe availability [*Martin and Fitzwater*, 1988; *Martin et al.*, 1994; *Coale et al.*, 1996; *Boyd et al.*, 2000]. Figure 5 shows the combined effects of shifting the floral composition in favor of diatoms and increasing the organic carbon production. As before, the diatom fraction saturates when the Si:N export ratio is down to 5. Thereafter the overall production is increased so as to restore the initial Subantarctic box silicic acid concentration. The enhancement in production is fueled by available nitrate, which becomes depleted when it can no longer keep up with increasing availability of silicic acid when the Si:N uptake ratio is reduced to 2.5. At this limit, atmospheric pCO_2 is down to 253 from 277 ppm. Most of the 24-ppm drawdown is due to the enhanced organic carbon pump, which

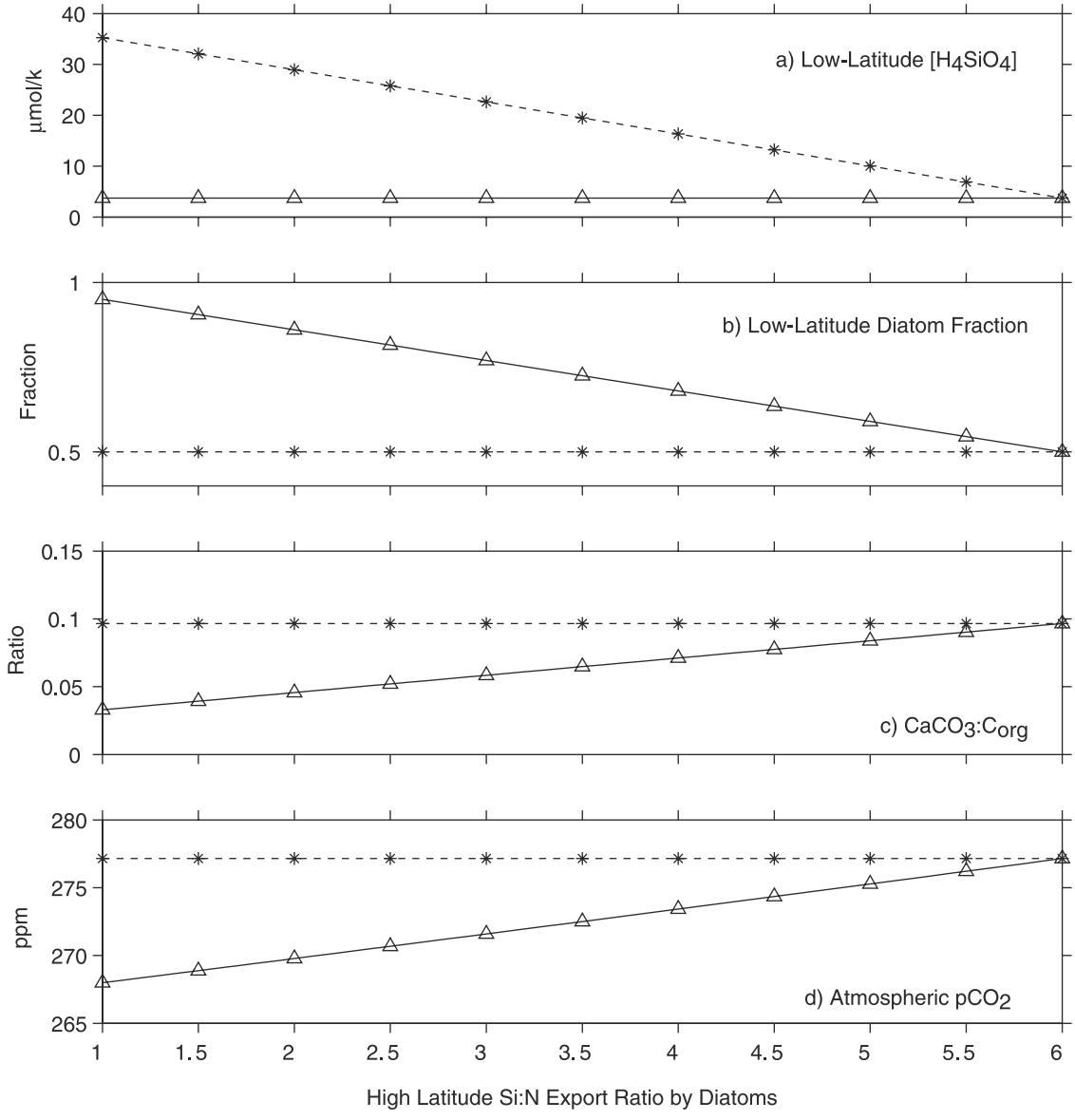

Figure 3. Silicic acid leakage reaching Low-Latitude surface box. Asterisks show model results when diatoms do not utilize excess silicic acid, which accumulates in Low-Latitude box, and when nothing else changes. Triangles indicate results when excess silicic acid in Low-Latitude box fuels diatom production at the expense of other phytoplankton. This causes (a) silicic acid to not accumulate, (b) diatom fraction to increase, (c) global $CaCO_3$:C_{org} ratio to drop, and (d) a drawdown in atmospheric CO_2. Interglacial control has Si:N ratio of 6.

was fueled by the 11.2 μmol kg^{-1} of nitrate that was initially in the Subantarctic box (Table 3). The effect of weakening the carbonate pump on atmospheric pCO_2 is 2 ppm, as before.

[31] A direct comparison between the 9-ppm drawdown (excess silicic acid leakage to the Low-Latitude box; see Figure 3) and the 24-ppm drawdown (leakage only to the Subantarctic box; see Figure 5) is not entirely valid, because the latter includes the effect of the organic carbon pump. We consider this latter effect in more detail in section 5.5. Here we point out that the CO_2 drawdown from carbonate pump alone in the eight-box model is very modest compared to the 80–100 ppm glacial/interglacial pCO_2 amplitude [*Barnola et al.*, 1987; *Petit et al.*, 1999].

5.2. Comparison With GCMs

[32] The atmospheric pCO_2 reduction achieved in section 5.1 is also only a small fraction of the 70-ppm drawdown that *Archer et al.* [2000a] obtained in their GCM. Although the mechanisms by which excess silicic acid was made more available to the low-latitude surface waters are distinct, the two experiments are essentially equivalent in that the forcing was a reduction in the low-latitude carbonate pump.

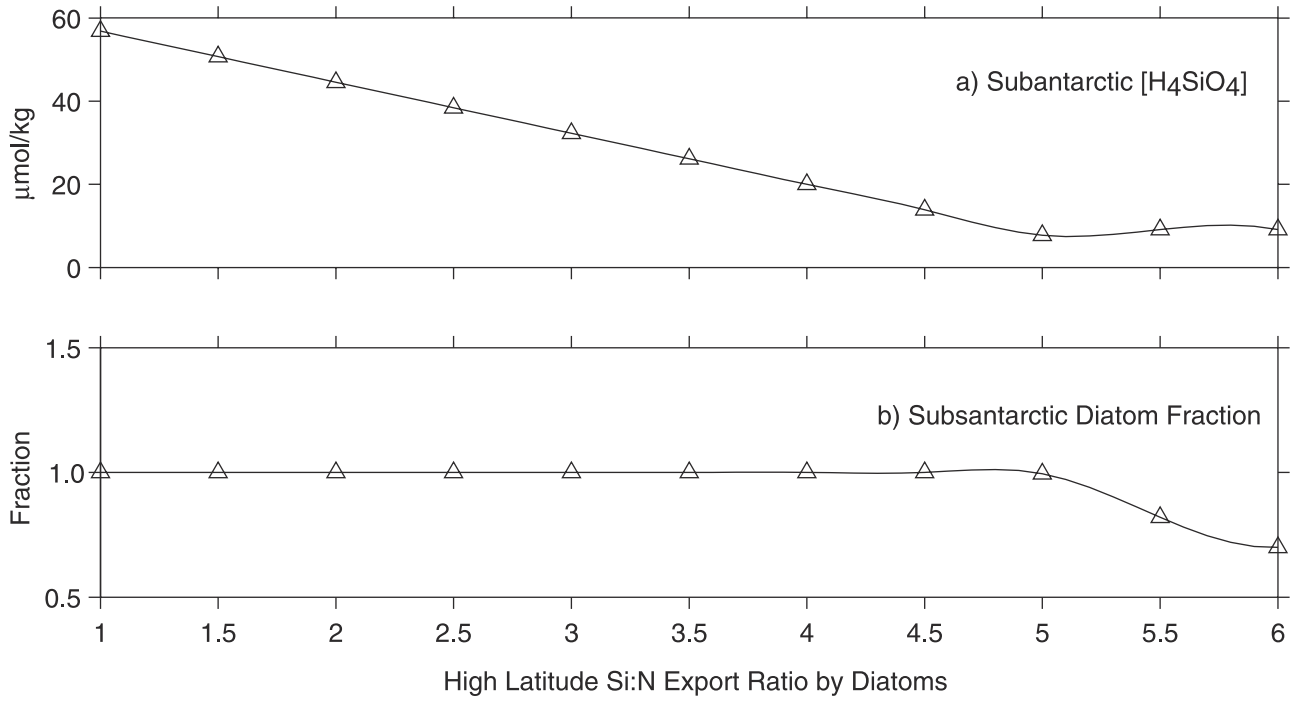

Figure 4. Silicic acid leakage reaching Subantarctic box with no change in overall organic carbon production (analogous to triangles in Figure 3). With increasing leakage, Subantarctic diatom fraction quickly saturates (Figure 4b) and silicic acid accumulates thereafter (Figure 4a). Interglacial control has Si:N ratio of 6.

[33] It has been suggested recently by *Broecker et al.* [1999] that GCMs have a larger pCO_2 response to changes in the temperature and nutrient dynamics in the low-latitude surface waters than simple box models. *Archer et al.* [2000b] argue that this is due to a more vigorous exchange of warm and cold surface waters in GCMs than in box models. Alternatively, the efficiency of air-sea gas exchange in polar surface waters ventilating the deep water and the contrast between preformed nutrient contents in NADW and Antarctic Bottom Water are perhaps more important (J.R. Toggweiler et al., Representation of the carbon cycle in box models and GCMs, 1, Solubility pump, submitted to *Global Biogeochemical Cycles*, 2001 (hereinafter referred to as Toggweiler et al., submitted manuscript, 2001); J.R. Toggweiler et al., Representation of the carbon cycle in box models and GCMs, 2, Organic carbon pump, submitted to *Global Biogeochemical Cycles*, 2001). It remains to be seen whether the real ocean behaves more like GCMs [*Archer et al.*, 2000b] or is somewhere in between box models and GCMs (Toggweiler et al., submitted manuscript, 2001).

[34] In order to test whether the small response that we observe relative to the *Archer et al.* [2000a] study is indeed due to GCM-box model difference, we have conducted an equivalent experiment with a recent version of the Princeton Ocean Biogeochemical Model (POBM) [*Gnanadesikan et al.*, 2002]. This model is based on the common biogeochemistry code of the Ocean Carbon Model Intercomparison Project [*Najjar and Orr*, 1999] that uses a low $CaCO_3$:C_{org} rain ratio suggested by *Yamanaka and Tajika* [1997]. The rain ratio at the bottom of the third layer of the POBM, representing the base of the mixed layer, is 0.07. To be consistent with the box model experiment, the $CaCO_3$ production in POBM was turned off completely in 80% of its ocean area. The 20% of the ocean area where calcite production was maintained is the far North Atlantic poleward of 60°N and the Southern Ocean poleward of 45°S. These two regions correspond to the four high-latitude surface boxes in the eight-box model.

[35] The $CaCO_3$ inhibition experiment in the Princeton model draws down atmospheric CO_2 by ~30 ppm over 3000 years (Figure 6). While pCO_2 is still decreasing slightly at 3000 years of simulation time, it is clear from the decreasing rate of drawdown that the equilibrium is not far off. The rain ratio of $CaCO_3$:C_{org} is reduced from 0.07 to 0.01. The CO_2 drawdown per unit change in the rain ratio for this model is thus ~500 ppm. When expressed in the same units, the 9-ppm drawdown in the eight-box model amounts to just 141 ppm. Thus, indeed, a significant difference exists between GCMs and simple box models in the sensitivity of atmospheric pCO_2 to changes in low-latitude nutrient dynamics [*Broecker et al.*, 1999].

[36] The difference in atmospheric CO_2 drawdown of ~30 ppm in POBM versus 70 ppm in the Hamburg model [*Archer et al.*, 2000a] stems partly from the fact that the latter was initialized with a much higher $CaCO_3$:C_{org} rain ratio. All else being equal, an initially higher rain ratio pumps alkalinity more strongly into deep waters to begin with and thus allows for a larger reduction in the carbonate pump and hence in the atmospheric pCO_2 (Figure 7). When the global $CaCO_3$:C_{org} rain ratio in the eight-box model is

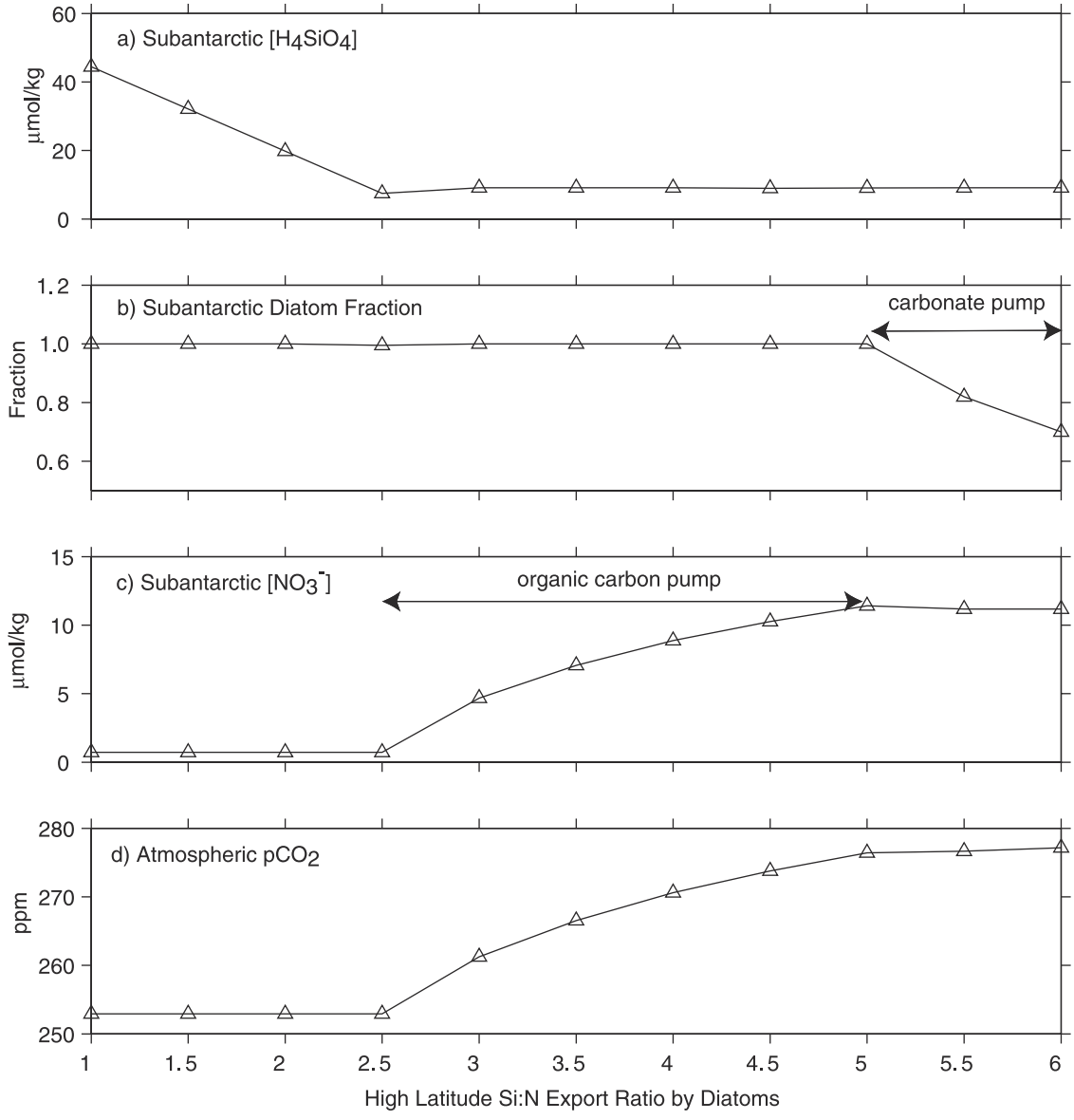

Figure 5. Silicic acid leakage reaching Subantarctic box with an increase in overall organic carbon production. Unlike in Figure 4, increased organic carbon production is fueled by available nitrate (Figure 5c) so as to utilize excess silicic acid (Figure 5a) after diatom fraction saturates (Figure 5b). Atmospheric CO_2 drawdown reflects both carbonate pump and organic carbon pump (Figure 5d). Interglacial control has Si:N ratio of 6.

reduced in the same manner as before, but with an initially higher ratio of 0.25, the atmospheric pCO_2 is now reduced by 35 instead of 9 ppm from the preindustrial 280 ppm. Nevertheless, this drop of 35 ppm is essentially equivalent to the 9-ppm drawdown when normalized to the $CaCO_3$:C_{org} rain ratio. These results are consistent with the pCO_2 response to the same forcing in the three-box model of *Toggweiler and Sarmiento* [1985] and in the seven-box model of *Toggweiler* [1999] (asterisks and crosses in Figure 7). The 16-box Cycling of Phosphorus in the Mediterranean (CYCLOPS) model also has a similar sensitivity [*Sigman et al.*, 1998; *Sigman and Boyle*, 2000]. This indicates that the pCO_2 sensitivity of the eight-box model is typical for a box model but is much lower than that for GCMs.

5.3. Carbonate Compensation

[37] Thus far we have only considered the effect of altering the strength of the carbonate pump on the atmospheric pCO_2. Here we consider the much larger effect of carbonate compensation [*Sigman et al.*, 1998]. A reduction of the global $CaCO_3$:C_{org} rain ratio by enhancing diatom export at the expense of nondiatoms diminishes calcite rain to the deep ocean. As a result, the riverine input of alkalinity would now exceed its removal by calcite burial. To restore

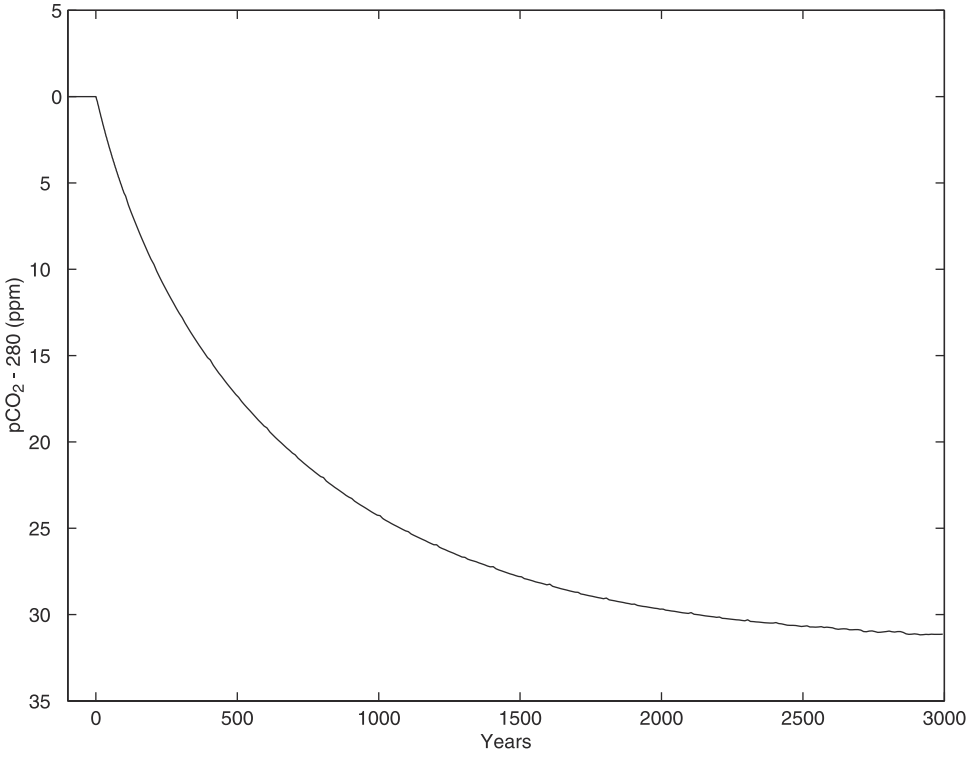

Figure 6. Atmospheric pCO_2 in Princeton Ocean Biogeochemistry Model (POBM) in response to inhibiting $CaCO_3$ production. $CaCO_3$:C_{org} rain ratio is set to zero in 80% of equatormost surface ocean.

the alkalinity balance, carbonate compensation in this case would tend to deepen the calcite lysocline, thus increasing the area of the seafloor where calcite is preserved. This will bury proportionally more calcite rain, so that even with a reduced calcite rain to the seafloor, the removal of alkalinity by calcite burial can balance its riverine input.

[38] There are two ways to simulate carbonate compensation in ocean carbon cycle models: "closed system" and "open system" [*Sigman et al.*, 1998]. In the former, the ocean-atmosphere system is "closed" with respect to alkalinity input and output. Sedimentary processes are ignored, and thus the calcite lysocline cannot be simulated. A closed system carbonate compensation simply restores the deep ocean carbonate ion to its initial concentration by increasing or decreasing the concentrations of alkalinity and ΣCO_2 in all the boxes uniformly in a 2:1 ratio [*Broecker and Peng*, 1987]. In our box model the atmospheric pCO_2 response to this compensation for the two cases of excess silicic acid leakage (i.e., leakage to the Low-Latitude box versus Subantarctic box) is quite modest (open symbols in Figure 8) compared to the CO_2 drawdown due carbonate pump effect alone (Figures 3d and 5d). The maximum compensation, achieved when the carbonate pump is most reduced (i.e., when Si:N export is down to 1 from the interglacial 6), is $\sim$5 ppm for both cases.

[39] An open system model accounts for the depth of the calcite lysocline by modeling the riverine input of alkalinity and sedimentary calcite dissolution and burial. When excess silicic acid leaks out only to the subantarctic, where both the carbonate pump and organic carbon pump operate (Figure 5), open system compensation draws down atmospheric CO_2 to 242 ppm (solid circles in Figure 8). Since the carbonate pump in the subantarctic was small to begin with, eliminating it does not result in a significant reduction in the global $CaCO_3$:C_{org} rain ratio and hence in calcite rain. Therefore the calcite lysocline is deepened by only 300 m. This modest deepening is also partly due to the increased organic carbon pump, which increases the calcite export associated with the increased overall production and counters the reduction in calcite export due to increased competition with diatoms.

[40] In the alternative case where excess silicic acid reaches the Low-Latitude box, open system compensation draws down atmospheric CO_2 to $\sim$230 ppm by the time the high-latitude Si:N export ratio is reduced to 3 from 6 (solid triangles in Figure 8). Unlike the previous case, this drawdown is accompanied by >1-km deepening in the calcite lysocline. The atmospheric pCO_2 predicted from simulations with even larger excess silicic acid leakage (i.e., Si:N export lower than 3) does not achieve a steady state. In this range, the surface calcite production is smaller than the riverine input, and therefore calcite burial can never match riverine input. With time, the saturation horizon and the calcite lysocline will reach the ocean floor, ocean alkalinity will continue to increase, and atmospheric pCO_2 will continue to decrease. This is consistent with the results from CYCLOPS, whose steady state lysocline deepened by >1 km in response to halving the global $CaCO_3$:C_{org} rain ratio from its initial value of 0.4 (see Appendix C). By contrast, *Archer et al.* [2000a] show that carbonate compensation of their +200% H_4SiO_4 model does not bring

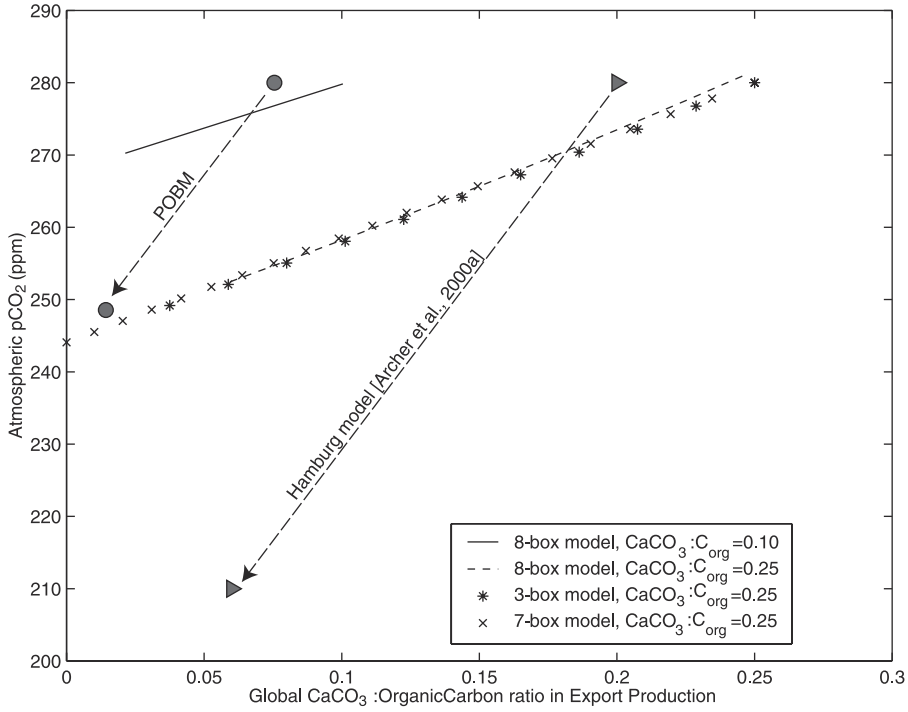

Figure 7. Atmospheric pCO_2 sensitivity to global particulate $CaCO_3$:C_{org} rain ratio. Solid line indicates eight-box model interglacial control (initial rain ratio of 0.1; see Figure 3d). Dashed line indicates the same experiment, except model was instead initialized with a rain ratio of 0.25. Initialization was accomplished by simply equilibrating 0.25-ratio model ocean with a 280-ppm atmosphere. In the process of equilibration the ocean-atmosphere system loses ~1% of total carbon inventory. Though not shown here, the result is nearly identical when model was tuned to new rain ratio, while preserving carbon inventory. Crosses and asterisks show results from three-box model [*Toggweiler and Sarmiento*, 1985] and from seven-box model [*Toggweiler*, 1999], respectively, that have initial rain ratio of 0.25. Circles indicate starting and ending states of POBM experiment, shown in Figure 6. Triangles show "uncompensated" Hamburg glacial model without land carbon transfer (268 ppm, rain $CaCO_3$:C_{org} of ~0.20) and +200% H_4SIO_4 model (198 ppm, rain ratio of ~0.06) [*Archer et al.*, 2000a]. Hamburg model results were shifted by +12 ppm so that starting pCO_2 is 280 ppm.

about such a large lysocline deepening. They suggest that the contrasting lysocline behavior between box models and GCMs may be due to differences in total organic matter production and to pCO_2 sensitivity to low-latitude forcing. They also note that when $CaCO_3$ production in their GCM is made spatially uniform so as not to distinguish the Atlantic and the Pacific, the large deepening of the lysocline in box models is observed, thus suggesting that the partitioning of $CaCO_3$ production between major ocean basins is critical.

[41] There are two important implications from these results. First, box models under the silicic acid leakage scenarios alone cannot simulate the full glacial atmospheric pCO_2 lowering. Even with the large amplification from open system carbonate compensation, only about half of the 80- to 100-ppm glacial-interglacial pCO_2 amplitude can be explained. This indicates that there is a limit to how much atmospheric pCO_2 can be reduced by increasing the silica inventory of the ocean by aeolian supply [*Harrison*, 2000] or riverine input [*Froelich et al.*, 1992]. According to box models the potential reduction is insufficient to account for the peak glacial pCO_2 levels.

[42] Second, the model predicts a very contrasting response of the lysocline depth to the two cases of excess silicic acid leakage. This offers an opportunity to evaluate these two cases in light of available paleo-lysocline evidence. Records of sedimentary $CaCO_3$ content suggest that the lysocline depth during the LGM was not significantly different from the modern [*Farrell and Prell*, 1989; *Catubig et al.*, 1998]. This is more consistent with the model lysocline response when silicic acid leakage only reaches the subantarctic. However, inferring past lysocline depth from bulk sedimentary $CaCO_3$ content is difficult, because it, alone, cannot distinguish the effects of calcite preservation and production. In fact, a calcite dissolution index based on the thickness of fossil foraminifera suggests that the carbonate ion concentration of the deep equatorial Pacific was ~20 μmol kg^{-1} higher during LGM than today [*Broecker et al.*, 2001; *Broecker and Clark*, 2001]. This would translate to more than a 1-km deepening of the calcite saturation horizon and hence of the lysocline. This sedimentary record would favor the model lysocline response when silicic acid reached all the way to the low-latitude surface waters. Paleoceanographic evidence thus appears

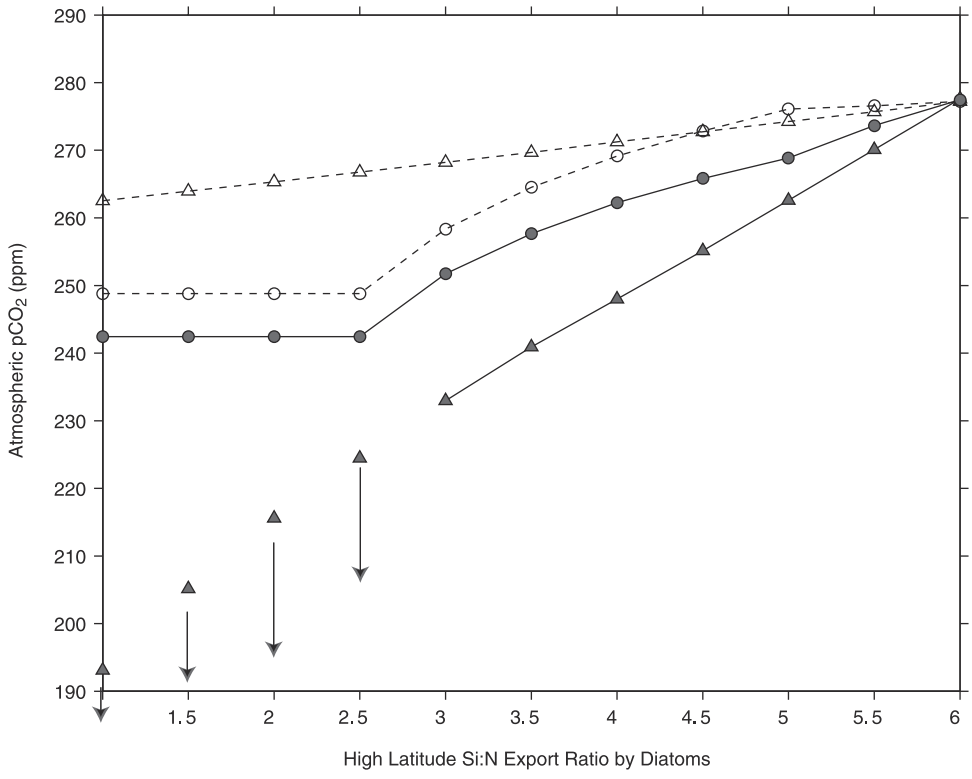

Figure 8. Effect of carbonate compensation on atmospheric pCO_2 in eight-box model. Open symbols show closed system carbonate compensation response. Solid symbols show open system response. Silicic acid leakage to Low-Latitude box is indicated by triangles. Leakage to Subantarctic box is shown by circles. For comparison, see Figures 3 and 5 for uncompensated simulations. Arrows indicate that these simulations will continue to draw down CO_2 with time, because the alkalinity budget cannot be balanced (see text and Appendix C). Interglacial control has Si:N ratio of 6.

inconclusive at this time with regard to the depth of the calcite lysocline during the LGM. Furthermore, sedimentary evidence for any significant change in paleo-lysocline depth, especially if short-lived, can be obscured subsequently by a change in the opposite direction.

5.4. Glacial Boundary Conditions

[43] Recent reviews by *Sigman and Boyle* [2000] and *Archer et al.* [2000a] make clear that the task of achieving peak glacial atmospheric pCO_2 levels is made more difficult with the addition of glacial boundary conditions. Here we briefly assess them in the eight-box model.

[44] Three glacial conditions taken together increase atmospheric pCO_2 from 277 to 293 ppm (Table 4). The first is a net transfer of carbon from land to ocean. The presence of large ice sheets over North America and Eurasia and of colder and drier climates that prevailed during glacial times are believed to have supported terrestrial biomes and soils that stored less carbon than during interglacial times. We take 500 Gt C for terrestrial carbon transfer as estimated by benthic foraminiferal $\delta^{13}C$ [*Shackleton*, 1977], although larger estimates of between 700 and 1350 Gt C have been made from terrestrial biome reconstruction [*Adams et al.*, 1990; *Crowley*, 1995]. The addition of 500 Gt C to the ocean increases ΣCO_2 relative to alkalinity and raises atmospheric pCO_2 by 42 ppm. Second, past sea level changes recorded in corals indicate that the LGM sea level was lower than today by ~120 m [*Fairbanks*, 1989], which represents ~3% of the average ocean depth. The effect of a 3% saltier ocean is to reduce the CO_2 solubility in seawater and thereby raise atmospheric pCO_2 in the model by an additional 7 ppm. The third effect is lower glacial sea surface temperatures, which increase the solubility of CO_2 in seawater. Available paleoceanographic evidence suggests that the cooling in low-latitude surface temperatures during LGM compared to the Holocene was between 2–3°C [*CLIMAP Project Members*, 1981; *Broecker*, 1986; *Rostek et al.*, 1993] and 5°C [*Stute et al.*, 1992; *Guilderson et al.*, 1994]. High-latitude surface temperatures were cooler by perhaps 3°C, as inferred from deep ocean cooling [*Shackleton*, 2000]. A cooling of 5°C in low latitudes and 3°C in high latitudes causes a reduction in the atmospheric pCO_2 of 33 ppm. These results, which were obtained here with the eight-box model, are consistent with those reported for the CYCLOPS model [*Sigman and Boyle*, 2000].

5.5. Stratification and Nutrient Depletion

[45] The potential importance of the Southern Ocean biological pump and stratification in controlling atmos-

Table 4. Glacial Boundary Conditions on Atmospheric pCO_2[a]

	Glacial Ocean	Atmospheric pCO_2, ppm
Interglacial control		277
Terrestrial carbon transfer	+500 Gt	+42
Salinity change	+3%	+7
SST change (high, low latitude)	−3°C, −5°C	−33
After glacial boundary conditions		293

[a] SST is sea surface temperature. High-latitude surface temperature cooling was modified in some boxes to stay above seawater freezing temperature.

pheric pCO_2 has been recognized by several groups [*Knox and McElroy*, 1984; *Sarmiento and Toggweiler*, 1984; *Siegenthaler and Wenk*, 1984] and has been a topic of numerous studies since. We revisit the topic here, because the silicic acid leakage scenario alone was shown in box models to be insufficient to account for the full glacial atmospheric pCO_2. Also, the increased Fe availability in the glacial Southern Ocean that we invoked to trigger silicic acid leakage is expected to enhance the overall biological production [*Martin and Fitzwater*, 1988; *Martin et al.*, 1994; *Coale et al.*, 1996; *Boyd et al.*, 2000]. Finally, we can use the eight-box model to examine how the two forcings affect the relative importance of nitrate and silicic acid as the limiting nutrient in the Southern Ocean over the previous glacial cycles [*Brzezinski et al.*, 2002].

[46] Figure 9 shows the response of the eight-box model to Southern Ocean stratification and export of organic

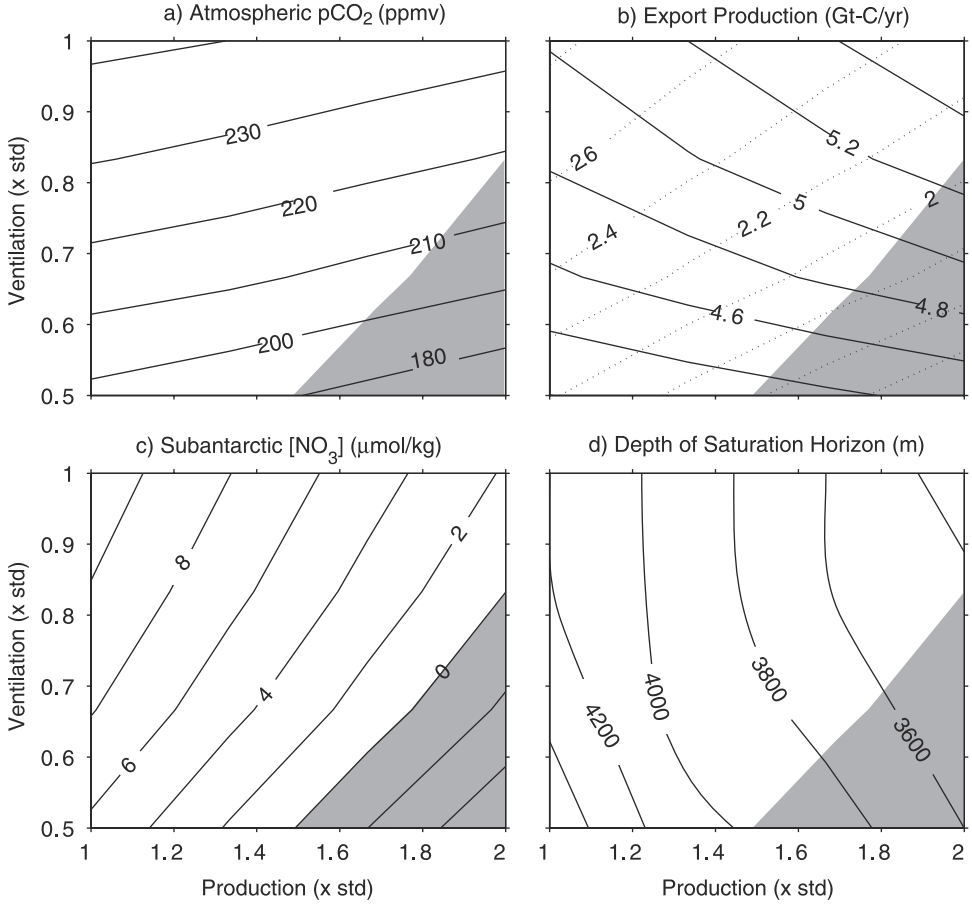

Figure 9. Eight-box model sensitivity to increased Southern Ocean stratification and export production. (a) Atmospheric pCO_2. (b) Organic carbon export (solid lines, global; dashed lines, Low-Latitude). (c) Nitrate concentration in Subantarctic box. (d) Depth of calcite saturation horizon in Deep box. Shading indicates where Subantarctic box nitrate concentration is negative. Ventilation fluxes *fcd* and *fpd* range between 50 and 100% of their interglacial values. Organic carbon export in Polar and Subantarctic boxes varies between 100 and 200% of their interglacial values. Base condition (i.e., ventilation × 1 and production × 1) is open system model with Southern Ocean Si:N export ratio of 3.5 with excess silicic acid reaching Low-Latitude box. Within entire parameter space shown, calcite production exceeds riverine input, so the ocean alkalinity budget can reach steady state. Nitrate and silicic acid in Low-Latitude box are restored to their initial concentrations.

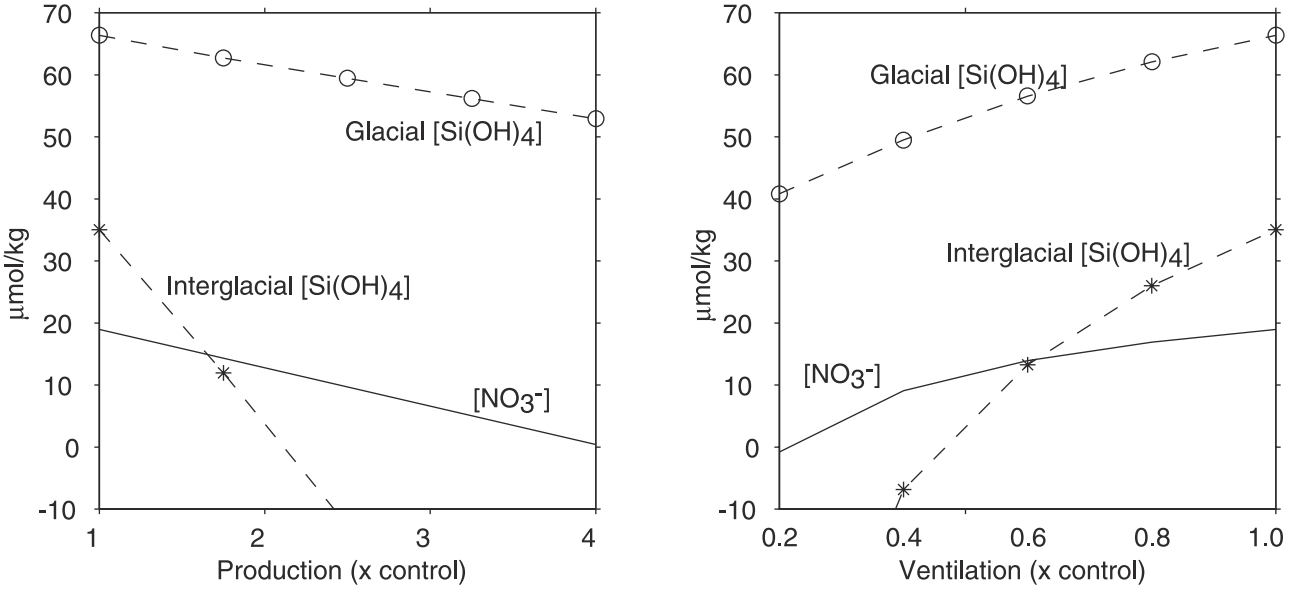

Figure 10. Polar box nitrate and silicic acid with and without silicic acid leakage under increased Southern Ocean production and stratification. Asterisks indicate "interglacial" silicic acid concentrations without silicic acid leakage (i.e., Si:N export ratio of 6). Circles indicate "glacial" silicic acid concentration with leakage (Si:N export ratio of 1). (left) Organic carbon export in the Polar and Subantarctic boxes varies between 100 and 400% and (right) ventilation fluxes *fcd* and *fpd* range between 20 and 100% of their respective interglacial values.

carbon production. Here the base condition (i.e., ventilation $\times$ 1 and production $\times$ 1) is the open system compensated model with a Southern Ocean Si:N export ratio of 3.5 with excess silicic acid reaching the Low-Latitude box (Figure 8). This state was chosen because stratification and nutrient depletion can be seen as additive effects on top of silicic acid leakage and open system carbonate compensation. The depth of the calcite lysocline for the base condition is 4050 m, down from 3000 m in the interglacial control (Appendix C).

[47] By increasing the Southern Ocean stratification and export organic carbon production, the model is able to achieve steady state atmospheric pCO_2 values comparable to those of peak glacial times (Figure 9a). However, the result is not meaningful in the parameter space, where the combination of the two forcings drives the nitrate stock in the Subantarctic box to negative values (Figure 9c). Where the subantarctic nitrate content is positive, atmospheric pCO_2 approaching the glacial value is predicted only when the Southern Ocean ventilation is reduced by approximately half the interglacial control. This space is characterized by a deepening of the calcite saturation horizon and hence of the lysocline by 1 km or more (Figure 9d). This is consistent with a lysocline deepening implied from calcite dissolution index based on the thickness of fossil foraminifera [*Broecker et al.*, 2001; *Broecker and Clark*, 2001] but is inconsistent with a relatively constant lysocline depth inferred from sedimentary $CaCO_3$ content [*Farrell and Prell*, 1989; *Catubig et al.*, 1998]. The lysocline is sensitive to changes in organic carbon production, because it can change the global calcite production to which the lysocline must adjust in order to balance calcite burial with riverine input. By contrast, deep ventilation by itself does not affect the lysocline, because calcite production is unaltered. Modest changes in the lysocline in response to stratification (i.e., decreased ventilation; see Figure 9d) reflects diminished organic carbon production (Figure 9b) and hence reflects diminished calcite production as a result of reduced upwelling supply of nutrients.

[48] Nitrate concentration in the Subantarctic box offered a useful constraint in determining a physically meaningful parameter space above, because in the model it was most susceptible to becoming completely depleted compared to nitrate in other boxes and to other nutrients in all boxes. The result was obtained for a Southern Ocean Si:N export ratio of 3.5. This is intermediate between the presumed interglacial value of 6 and a presumed upper limit of 1, which is about the Si:N molar ratio in nutrient-replete diatoms living today in low latitudes [*Brzezinski*, 1985]. When export Si:N ratio is larger than 3.5 (i.e., more preferential utilization of silicic acid approaching the modern condition), silicic acid is more susceptible to becoming depleted in the Southern Ocean under both enhanced production and stratification (asterisks in Figure 10). When Si:N export ratio is smaller (approaching our presumed glacial conditions), silicic acid is less preferentially used and becomes more abundant (circles in Figure 10). Nitrate therefore becomes relatively more scarce and susceptible to getting depleted under the presumed glacial conditions. This result is consistent with sedimentary $\delta^{30}Si$ and $\delta^{15}N$ measurements from Antarctic sediments that indicate an availability of silicic acid and nitrate in the opposite sense during glacial times versus interglacial times [*Francois et al.*, 1997; *De La Rocha et al.*, 1998; *Brzezinski et al.*, 2002].

6. Discussion and Conclusions

[49] We are unable to distinguish the two possible destinations of the excess silicic acid that we assumed was created during the LGM in Antarctic surface waters to the south of the modern Polar Front. Any significant consumption of the silicic acid in the subantarctic surface waters just to the north would require an enhanced organic carbon pump, since the fraction of diatoms to the total production saturates quickly (Figures 4 and 5). If, instead, much of the consumption occurs in the low-latitude surface waters, a shift of the phytoplankton species composition in favor of diatoms alone is sufficient to consume nearly all excess silicic acid (Figure 3). While the two cases predict contrasting behavior of the calcite lysocline depth, available sedimentary studies that bear on the deep carbonate ion content during LGM [*Farrell and Prell*, 1989; *Catubig et al.*, 1998; *Broecker et al.*, 2001; *Broecker and Clark*, 2001] appear unable to distinguish between the two at this time. Since they are not mutually exclusive, perhaps the two cases in some combination may have operated at the same time. In any case, open system compensation in the simple box model can only reduce the steady state atmospheric pCO_2 by $\sim$40–50 ppm from the interglacial value (Figure 8). Peak glacial values of 180–200 ppm can be achieved when Southern Ocean stratification is increased, in addition to carbonate pump reduction and open system compensation (Figure 9). Southern Ocean nutrient depletion can also effectively draw down atmospheric CO_2, but nitrate in the Subantarctic box becomes depleted before glacial pCO_2 values can be achieved.

[50] By contrast to simple box models, the atmospheric pCO_2 in GCMs has a much higher sensitivity to reduced carbonate pump (Figure 7). By reducing the global $CaCO_3$:C_{org} rain ratio from an initial value of 0.1, GCMs can reduce atmospheric CO_2 by $\sim$50 ppm without having to enhance either Southern Ocean production or ventilation. Open system compensation would further draw down CO_2 from the atmosphere [*Archer et al.*, 2000a]. If the sensitivity of the real atmospheric pCO_2 is better represented by GCMs than by box models [*Archer et al.*, 2000a], then the proposed silicic acid leakage mechanism by itself can be a viable explanation for the low glacial atmospheric pCO_2.

[51] The changes in the relative utilization efficiency of nitrate versus silicic acid predicted by this mechanism (Figure 10) are consistent with $\delta^{30}Si$ and $\delta^{15}N$ measurements from the Antarctic sediments [*Francois et al.*, 1997; *De La Rocha et al.*, 1998; *Brzezinski et al.*, 2002]. Elevated opal accumulation rates in the subantarctic sediments of the Atlantic and Indian sectors during LGM [*Kumar et al.*, 1995; *Francois et al.*, 1997; *Anderson et al.*, 2002] are consistent with silicic acid leakage to the subantarctic. A comparatively lower opal accumulation in the glacial subantarctic Pacific [*Chase et al.*, 2002] as well as a larger marine silica inventory during the LGM than today are both consistent with leakage out of the Southern Ocean. Like *Harrison* [2000], we assume that any significant leakage of excess silicic acid to low-latitude surface waters would enhance the production of diatoms at the expense of other phytoplankton. However, sedimentary evidence for increased opal burial in the low latitudes is lacking. This does not necessarily weaken the proposed silicic acid leakage mechanism, because the sedimentary preservation of opal is not related to its production in any obvious way in large parts of the modern ocean [*Nelson et al.*, 1995].

[52] Finally, we note that we have assumed, as previous studies have done, that glacial atmospheric pCO_2 was in steady state. The steady state assumption is extremely useful and common in paleoclimatological studies. However, justification for it in many cases appears to be either inadequate or lacking altogether. An inspection of the Vostok atmospheric pCO_2 record, for example, clearly shows that minimum values occur only during peak glacial periods [*Petit et al.*, 1999]. These periods last perhaps 10,000 years, a relatively short time compared to the 100,000 years that characterize the late-Pleistocene glacial-interglacial cycle. The 10,000-year duration is also roughly comparable to the residence time of carbonate ions in the ocean and hence to the timescale of carbonate compensation [*Broecker and Peng*, 1982]. Therefore the steady state assumption with regard to peak glacial atmospheric pCO_2 may not be entirely valid. This has very important implications for studies such as this. If peak glacial atmospheric pCO_2 represents only a transient event, even box models can achieve glacial pCO_2 values with a reduction in carbonate pump combined with open system carbonate compensation without having to call for an enhanced high-latitude stratification and nutrient depletion (Figure 8). Furthermore, a short event may not leave behind a sedimentary record.

Appendix A: Carbon Isotope Fractionation in Eight-Box Model

[53] The carbon isotope content of the ocean and atmosphere in the model is expressed as pseudoconcentrations [*Craig*, 1969]. It is the fractional deviation of isotopic ratios of the sample from the reference (i.e., $1 + \delta^{13}C/1000$ and $1 + \Delta^{14}C/1000$), weighted by the abundance of their carrier, which is ΣCO_2 in the ocean and pCO_2 in the atmosphere. Since pseudoconcentrations are converted back to the usual $\delta^{13}C$ and $\Delta^{14}C$ notations, the isotopic ratio of the reference never enters the calculation [*Toggweiler and Sarmiento*, 1985].

[54] Discrimination against ^{13}C during marine photosynthesis is assumed to be -23‰ with respect to $\delta^{13}C$ of the ambient ΣCO_2. The total ^{13}C fractionation in air-sea gas exchange accounts for a small kinetic fractionation, the air-to-sea isotope flux, and the sea-to-air isotope flux [*Siegenthaler and Munnich*, 1981]. The magnitude of these isotope fractionations is dependent on temperature. The kinetic fractionation factor is very weakly dependent on temperature [*Zhang et al.*, 1995]. The air-to-sea isotope flux is driven by atmospheric pCO_2, and the equilibrium fractionation factor between gaseous and aqueous CO_2 is from *Vogel et al.* [1970]. The sea-to-air isotope flux is driven by the surface ocean pCO_2 and accounts for the isotope equilibration between CO_2 and the three species of ΣCO_2. The gaseous CO_2-aqueous CO_2 fractionation factor is from *Vogel et al.* [1970], the aqueous CO_2–HCO_3^- fractionation factor is from *Mook et al.* [1974], and the aqueous CO_2–$CO_3^=$ is from *Zhang et al.* [1995]. The total sea-to-air isotope

Table B1. Inverse Model Priors, Solutions, and Uncertainty[a]

	Priors	Solutions	Uncertainty			
			A Priori	A Posteriori	Monte Carlo	Total
		Water Fluxes (Sv)				
T	20.0	11.2	100.0	73.5	10.4	74.2
fcd	20.0	28.9	100.0	59.1	7.4	59.6
fcp	20.0	14.3	100.0	84.4	7.1	84.7
fpd	20.0	18.0	100.0	47.8	8.6	48.6
fps	20.0	21.3	100.0	82.6	12.6	83.6
fsl	20.0	9.0	100.0	58.1	8.9	58.8
flm	60.0	54.9	100.0	58.0	10.2	58.9
fln	20.0	0.8	100.0	64.0	7.9	64.5
fna	20.0	10.0	100.0	71.4	6.7	71.7
fmd	20.0	5.6	100.0	37.0	2.8	37.1
fma	20.0	7.9	100.0	69.8	4.5	69.9
fad	20.0	2.0	100.0	39.2	3.9	39.4
		Production (Gt C yr^{-1})				
Continental Margin	0.70	0.47	10.00	1.26	0.17	1.27
Polar	0.70	0.53	10.00	1.48	0.14	1.49
Subantarctic	0.70	0.54	10.00	1.40	0.18	1.41
North	0.70	0.65	10.00	1.36	0.19	1.37
Low-Latitude	2.77	2.84	10.00	1.83	0.18	1.84

[a] Sv = 10^6 m^3 s^{-1}; Gt C yr^{-1} = 10^{15} g organic carbon per year. For comparison with 20-Sv water flux prior estimate, a recent radiocarbon-derived estimate of NADW formation rate is ~15 Sv [*Broecker et al.*, 1998]. It is also consistent with an analysis of Southern Ocean oxygen content that indicates an average upwelling rate of 45 m yr^{-1} [*Gordon and Huber*, 1990]. The 60-Sv prior estimate for flux *flm* alone is much larger than the rest, because model simulations consistently show that a large *flm* is necessary to sufficiently ventilate the deep ocean and yield a reasonable preindustrial atmospheric Δ^{14}C. As for production terms, magnitude of their prior estimates is based on inversion results without prior estimates. Regional breakup is based on satellite-derived estimates of new production as summarized by *Gnanadesikan et al.* [2002].

flux is represented by their sum, weighted by their relative abundance, which is calculated from alkalinity and ΣCO_2 concentrations. Fractionation for ^{14}C is assumed to be mass dependent. The fractionation factors for ^{13}C are exactly doubled for radiocarbon.

Appendix B: Inverse Model

[55] Eight variables (silicic acid, nitrate, oxygen, potential temperature, alkalinity, ΣCO_2, δ^{13}C, and Δ^{14}C) in eight boxes give a total of 64 conservation equations. However, the temperature equations are neglected entirely, because it has been shown that a box model tuned to fit an observed temperature distribution is inconsistent with the same model tuned to fit the distribution of other types of tracers [*Siegenthaler and Joos*, 1992]. Apparently, the manner by which heat enters the ocean and is transported within it is different than how oceanic CO_2, for example, exchanges with the atmosphere and is transported. We also neglect the oxygen equations, which are redundant to the nitrate equations. Finally, the δ^{13}C equations are neglected, because their typical fractional deviation from the sample in the ocean is so small that when expressed as pseudoconcentrations (Appendix A), they become very similar to the ΣCO_2 equations. The 36 equations, with their time-differential terms set to zero for steady state, are then inverted to solve for the 12 water fluxes and for the five export production fluxes for each of the surface boxes (Table B1). The solution to the inverse model minimizes the mismatch between the ''observations'' (Table 2) and steady state model predictions in the least squares sense.

[56] In the system of linear equations expressed as $\mathbf{Ax} = \mathbf{b}$, the inversion matrix $\mathbf{A}$ thus has a dimension of 36×17. Its rows correspond to 36 equations and the columns correspond to the 17 unknowns. The elements of vector $\mathbf{b}$ correspond to the constants or observations for the 36 steady state equations. With more constraints than unknowns, the problem is formally overdetermined and is solved by singular value decomposition for the solution vector x [*Press et al.*, 1992].

[57] Two important modifications were made to matrix $\mathbf{A}$. The first is a normalization of nutrient conservation equations by their remineralization stoichiometry. Without it, equations for ΣCO_2, for example, would be weighted more than seven times (117/16) the equations for nitrate. Normalization removes these biased weights. The second is a slight modification of the target surface ΣCO_2 concentrations from the observed values, because the combination of observed surface alkalinity and ΣCO_2 concentrations is not in equilibrium with the preindustrial 280-ppm atmosphere. Modification is made so that the surface ocean would be in equilibrium with an atmospheric pCO_2 of 280 ppm.

[58] The condition number of matrix $\mathbf{A}$ thus constructed is just about 3000. The inversion solution obtained without any means of regularization is for the most part reasonable, except for slightly negative water fluxes *fln*, *fmd*, and *fma* and a negative production in the Polar box. The last two water fluxes allow the Middle box to communicate directly with the two deeper boxes (Figure 1). An examination of the target nutrient concentrations in Table 2 makes it clear that the two fluxes must be small. Otherwise, the Middle box would not be able to maintain its much higher temperature and lower nutrient concentrations compared to the Atlantic and Deep boxes.

[59] To obtain a more reasonable set of solutions, we regularize the set of equations by constraining the solution

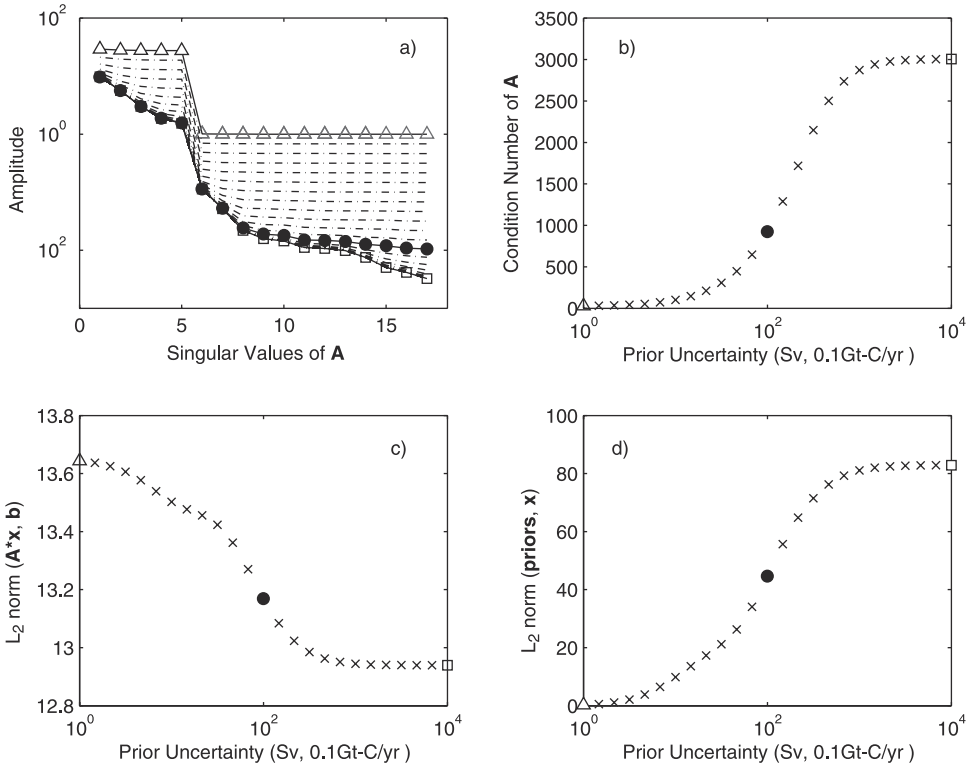

Figure B1. Sensitivity of the inversion to the strength of prior estimates. Selected properties shown as a function of how strongly inverse model solutions are to their prior estimates. (a) Spectra of 17 singular values, corresponding to five surface productions and 12 water fluxes. (b) Condition number of inversion matrix **A**. (c) Difference between observations and their reconstruction from inverse model solutions, expressed as L2 norm (i.e., a distance from observations vector **b** to product of **A** and solutions vector **x**). (d) Difference between inverse model solutions and their prior estimates. Triangles show strongest constraint (i.e., zero uncertainty in prior estimates). Squares indicate least constraint or largest a priori uncertainty (10,000 Sv for each of the water fluxes, and 100 Gt C yr^{-1} production for each of five surface boxes). Ideal set of solutions (circles) lies somewhere in between minimum and maximum constraints. Note log scales.

to a set of prior estimates of the solutions (hereafter "priors") and by truncating very small singular values [*Press et al.*, 1992]. Priors are essentially the first guess of the solutions. We constrain the solutions as little as possible to the priors by assigning a large a priori uncertainty.

[60] A sensitivity study of the inversion solutions to the strengths of their priors suggests that the appropriate a priori error be ~100 Sv for the water fluxes and 10 Gt C yr^{-1} for production terms (Figure B1). Here the equations are inverted without singular value truncation, with the uncertainties of the circulation and production priors ranging from 0 Sv and 0 Gt C yr^{-1} (minimum uncertainties) to 10,000 Sv and 100 Gt C/yr^{-1} (maximum uncertainties). At their maximum the uncertainties are so large that the priors are meaningless, and the solutions thus obtained are equivalent to those inverted without priors, and the spectrum of singular values has the largest slope (squares in Figure B1a). The ratio of the maximum and minimum singular values gives the condition number, which is 3000, as we expect (square in Figure B1b). The solutions, using these large uncertainties, that agree with the observations to the greatest extent are least similar to the priors (squares in Figures B1c and B1d). As the prior uncertainties are reduced, solutions are increasingly constrained to their priors. The singular value spectrum becomes more flat, indicating the introduction of increasingly biased information, and the condition number becomes smaller. When the prior uncertainty is zero (i.e., no uncertainty), the solutions are exactly the same as the priors, meaning that no information from the 36 conservation equations has been utilized. The ideal set of solutions lies somewhere between the two extremes (circles in Figure B1). We selected a prior uncertainty of 100 Sv for water fluxes and 10 Gt C yr^{-1} for production terms. At these levels the a priori uncertainties are sufficiently large that the overall fit to the target is not significantly sacrificed (Figure B1c), and the priors solutions are not very similar to their priors (Figure B1d). A posteriori errors computed for this case show that they are smaller than the a priori errors (Table B1).

[61] We have also estimated the errors of the inverse model solutions that are associated with the inversion matrix **A** (i.e., uncertainties with the "observed" preindustrial state of the ocean and atmosphere). In a Monte Carlo simulation each element of matrix **A** was randomly perturbed by magnitudes equal to or smaller than the standard deviations of the mean observed values (Table 2). The standard deviations of 5000 such simulations indicate the

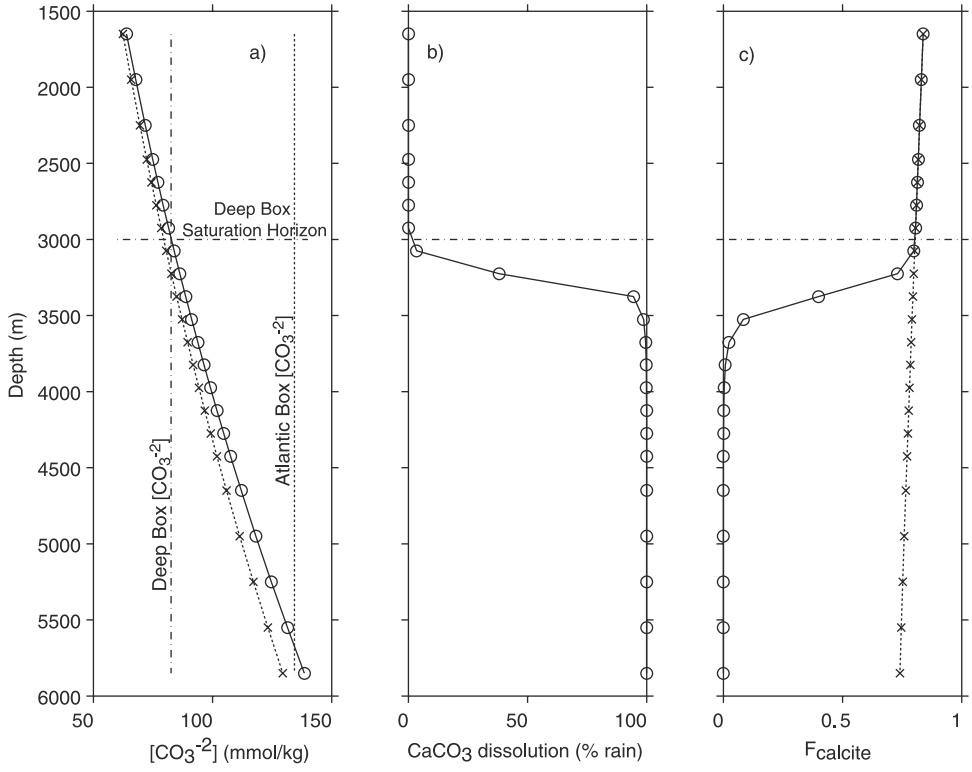

Figure C1. Sediment model properties for interglacial control. Depth profiles of (a) theoretical carbonate ion concentration at saturation with mineral calcite, (b) calcite dissolution (as percentage of calcite rain that reaches seafloor), and (c) sedimentary calcite fraction. In Figure C1a, vertical lines show "bottom water" carbonate ion concentrations in Deep and Atlantic boxes. Intersection of saturation and bottom water concentrations define saturation horizon, indicated with a horizontal dash-dotted line. Deep box profile is indicated by circles, and Atlantic box profile is indicated by crosses.

errors associated with matrix **A**. They are typically an order of magnitude smaller than the a posteriori errors (Table B1).

[62] Finally, we note that this inversion problem is not as overdetermined as the dimension of matrix **A** implies, because the nutrient conservation equations are not entirely mutually orthogonal. They are related to one another by the stoichiometric and export production ratios. It is also worth noting that while the production and circulation parameters obtained by inversion are more self-consistent than a set of parameters arbitrarily obtained by "hand-tuning," the former set of parameters is no more "true" than the latter set. Many processes simply cannot be represented realistically in box models and therefore have no truly meaningful oceanographic counterparts in reality.

Appendix C: Sediment Model

[63] Calcite dissolution is based on the bottom water-driven dissolution (d) parameterization of *Sigman et al.* [1998]:

$$d = 20.36 \times 10^{12}\left([CO_3^{=}]_{saturation} - [CO_3^{=}]_{bottomwater}\right)^{2.35} \cdot \sqrt{F_{calcite}},$$

where dissolution is given in units of μmol $CaCO_3$ cm^{-2} yr^{-1}. Saturation and bottom water carbonate ion concentrations are in units of mol kg^{-1}. $F_{calcite}$ is the fraction of calcite in the sediment mixed layer. As described in detail by *Sigman et al.* [1998], this formulation does not account for respiratory calcite dissolution and is based on output of the explicit sediment geochemistry model of *Martin and Sayles* [1996] using a calcite dissolution rate constant of 30 day^{-1} [*Keir*, 1980].

[64] This dissolution formulation is applied in the eight-box model to deep-sea sediments below 1500 m, which represents nearly 90% of the total area below the sea level. The sediments are divided into 22 depth ranges, whose bioturbated or sediment mixed layers are represented by well-mixed sediment bins that are coupled to the Atlantic and Deep boxes. The area and hence the size of each bin is determined from ocean hypsometry. The bottom water carbonate ion concentrations are those calculated for the two deep boxes by the model. The saturation concentration at each bin depth is calculated using the apparent solubility product of calcite in seawater at 1 atm pressure [*Ingle et al.*, 1973] modified to account for temperature and pressure effects [*Millero*, 1995].

[65] Figure C1 shows the steady state sedimentary calcite properties of the eight-box model coupled with the calcite dissolution model for the interglacial control. The saturation carbonate ion concentration increases with depth as pressure increases in both the Atlantic and Deep boxes

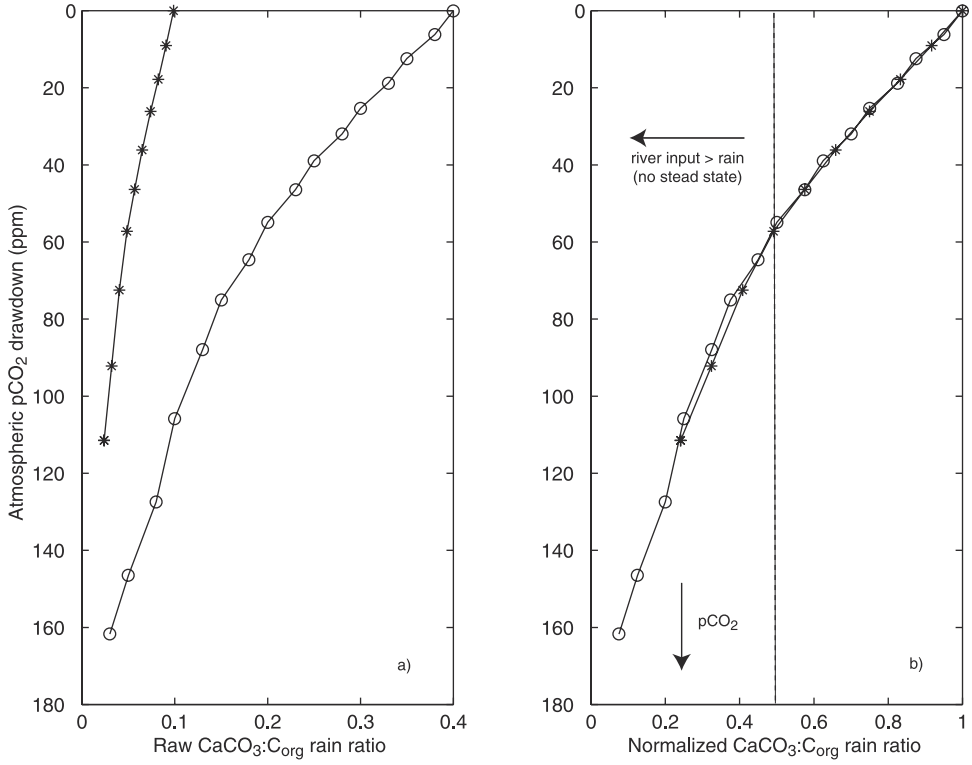

Figure C2. Open systems of eight-box model and Cycling of Phosphorus in the Mediterranean model [*Sigman et al.*, 1998]. Atmospheric CO_2 drawdown by two models in response to reduced global $CaCO_3$:organic carbon rain ratios with (a) raw ratio and (b) ratio normalized by its initial value. Total drawdown includes modest effect due to a weakened carbonate pump, which redistributes oceanic alkalinity, and much larger effect due to open system carbonate compensation.

(Figure C1a). The slightly higher saturation concentration for the Deep box is due to its lower temperature. The intersection of the theoretical saturation profile and predicted carbonate ion concentration of the two boxes defines the calcite saturation depth, which for the Deep box is 3000 m (horizontal dash-dotted lines in Figure C1). The Atlantic box is supersaturated at all depths and therefore has no saturation horizon. The calcite particles that reach the seafloor (i.e., $CaCO_3$ export minus water column remineralization) are mixed into the sediments and are subject to dissolution according to the above formulation. No sedimentary dissolution occurs above the saturation horizon in supersaturated waters. Most calcite rain dissolves in sediments bathed by undersaturated waters below the saturation horizon, with a transition zone of ~500 m (Figure C1b). The sedimentary calcite fraction drops precipitously below the saturation horizon (Figure C1c). This transition, occurring at ~3500 m in the model, indicates the calcite lysocline and is consistent with the depth of calcite lysocline of the modern ocean. These model results are all consistent with those shown by *Sigman et al.* [1998].

[66] As shown in Figure C2, the atmospheric pCO_2 response of the eight-box model and the CYCLOPS model [*Sigman et al.*, 1998] to a combination of a weakened low-latitude carbonate pump and an open system carbonate compensation also agrees. The CYCLOPS result shown here was obtained from the model with a much higher initial $CaCO_3$:organic carbon rain ratio than the eight-box model and includes the effect of respiratory calcite dissolution [*Sigman et al.*, 1998]. Normalization of the rain ratio is necessary for meaningful comparison, because the two models have different starting ratios. Assuming that the two models have comparable ocean hypsometry, normalization ensures that the same fractional change in the carbonate pump strength produces similar lysocline responses. It is important to note that when calcite rain falls below the riverine input, steady state cannot be reached. Even when the calcite lysocline reaches the bottom of the seafloor, removal of calcite from the ocean by burial will not be able to match the riverine input. In this case the ocean inventory of alkalinity and ΣCO_2 will continue to rise, and atmospheric pCO_2 will continue to fall. This limit is reached when the normalized, low-latitude $CaCO_3$:organic-C rain ratio is reduced by approximately half (Figure C2b).

[67] **Acknowledgments.** We thank A. Gnanadesikan, N. Gruber, and R. Toggweiler for discussions at various stages of preparing this manuscript. R. Key provided access to available WOCE data. Discussions about the inverse model with D. Baker, S.-M. Fan, and A. Jacobson were very helpful. D. Sigman kindly explained his sediment model. R.D. Slater ran POBM simulation. Finally, reviews by R.F. Anderson and D. Archer measurably improved the manuscript. This research was supported by

NSF grants OCE-9819144 and OCE-0097316 and by National Oceanic and Atmospheric Administration OGP support for the Carbon Modeling Consortium.

References

Adams, J. M., H. Faure, L. Faure-Denard, J. M. McGlade, and F. I. Woodward, Increases in terrestrial carbon storage from the Last Glacial Maximum to the present, *Nature*, *348*, 711–714, 1990.

Anderson, L. A., and J. L. Sarmiento, Redfield ratios of remineralization determined by nutrient data analysis, *Global Biogeochem. Cycles*, *8*(1), 65–80, 1994.

Anderson, R. F., Z. Chase, M. Q. Fleisher, and J. Sachs, The Southern Ocean's biological pump during the Last Glacial Maximum, *Deep Sea Res., Part II*, *49*, 1909–1938, 2002.

Archer, D., A. Winguth, D. Lea, and N. Mahowald, What caused the glacial/interglacial atmospheric pCO_2 cycles?, *Rev. Geophys.*, *38*(2), 159–189, 2000a.

Archer, D. E., G. Eshel, A. Winguth, W. Broecker, R. Pierrehumbert, M. Tobis, and R. Jacob, Atmospheric pCO_2 sensitivity to the biological pump in the ocean, *Global Biogeochem. Cycles*, *14*(4), 1219–1230, 2000b.

Bainbridge, A. E., GEOSECS Atlantic Ocean Expedition, in *Hydrographic Data 1972–1973*, 121 pp., Natl. Sci. Found., Washington, D. C., 1981.

Barnola, J. M., D. Raynaud, Y. S. Korotkevich, and C. Lorius, Vostok ice core provides 160,000-year record of atmospheric CO_2, *Nature*, *329*, 408–414, 1987.

Behrenfeld, M., and P. G. Falkowski, Photosynthetic rates derived from satellite-based chlorophyll concentration, *Limnol. Oceanogr.*, *42*(1), 1–20, 1995.

Belkin, I. M., and A. L. Gordon, Southern Ocean fronts from the Greenwich meridian to Tasmania, *J. Geophys. Res.*, *101*(C2), 3675–3696, 1996.

Boyd, P. W., et al., A mesoscale phytoplankton bloom in the polar Southern Ocean stimulated by iron fertilization, *Nature*, *407*, 695–702, 2000.

Brewer, P. G., A. L. Bradshaw, and R. T. Williams, Measurements of total carbon dioxide and alkalinity in the North Atlantic Ocean in 1981, in *The Global Carbon Cycle: Analysis of the Natural Cycle and Implications of Anthropogenic Alterations for the Next Century*, edited by D. Reichle, pp. 358–381, Springer Verlag, New York, 1986.

Broecker, W. S., Ocean chemistry during glacial time, *Geochim. Cosmochim. Acta*, *46*, 1689–1705, 1982.

Broecker, W. S., Oxygen isotope constraints on surface ocean temperatures, *Quat. Res.*, *26*, 121–134, 1986.

Broecker, W. S., and E. Clark, Glacial-to-Holocene redistribution of carbonate ion in the deep sea, *Science*, *294*, 2152–2154, 2001.

Broecker, W. S., and E. Maier-Reimer, The influence of air and sea exchange on the carbon isotope distribution in the sea, *Global Biogeochem. Cycles*, *6*(3), 315–320, 1992.

Broecker, W. S., and T.-H. Peng, *Tracers in the Sea*, Eldigio, Palisades, New York, 1982.

Broecker, W. S., and T.-H. Peng, The role of $CaCO_3$ compensation in the glacial to interglacial atmospheric CO_2 change, *Global Biogeochem. Cycles*, *1*(1), 15–29, 1987.

Broecker, W. S., D. Spencer, and H. Craig, GEOSECS Pacific Ocean Expedition, in *Hydrographic Data 1973–1974*, 137 pp., Natl. Sci. Found., Washington, D. C., 1982.

Broecker, W. S., et al., How much deep water is formed in the Southern Ocean?, *J. Geophys. Res.*, *103*(C8), 15,833–15,843, 1998.

Broecker, W., J. Lynch-Stieglitz, D. Archer, M. Hofmann, E. Maier-Reimer, O. Marchal, T. Stocker, and N. Gruber, How strong is the Harvardton-Bear constraint?, *Global Biogeochem. Cycles*, *13*(4), 817–820, 1999.

Broecker, W. S., R. F. Anderson, E. Clark, and M. Fleisher, Record of seafloor $CaCO_3$ dissolution in the central equatorial Pacific, *Geochem. Geophys. Geosyst.*, *2*, 10.1029\2000GC000151, 2001.

Brzezinski, M. A., The Si:C:N ratio of marine diatoms: Interspecific variability and the effect of some environmental variables, *J. Phycol.*, *21*, 347–357, 1985.

Brzezinski, M. A., D. M. Nelson, V. M. Franck, and D. E. Sigmon, Silicon dynamics within an intense diatom bloom in the Pacific sector of the Southern Ocean, *Deep Sea Res., Part II*, *48*, 3997–4018, 2001.

Brzezinski, M. A., C. J. Pride, D. M. Sigman, J. L. Sarmiento, K. Matsumoto, N. Gruber, G. H. Rau, and K. H. Coale, A switch from $Si(OH)_4$ to NO_3^- depletion in the glacial Southern Ocean, *Geophys. Res. Lett.*, *29*, 10.1029/2001GL014349, in press, 2002.

Catubig, N. R., D. E. Archer, R. Francois, P. deMenocal, W. Howard, and E.-F. Yu, Global deep-sea burial rate of calcium carbonate during the Last Glacial Maximum, *Paleoceanography*, *13*(3), 298–310, 1998.

Chase, Z., R. F. Anderson, M. Q. Fleisher, and P. Kubik, Accumulation of biogenic and lithogenic material in the Pacific sector of the Southern Ocean during the past 30,000 years, paper presented at Ocean Sciences Meeting, AGU, Honolulu, 2002.

CLIMAP Project Members, Seasonal reconstructions of the Earth's surface at the Last Glacial Maximum, *Map Chart MC-36*, Geol. Soc. of Am., Boulder, Colo., 1981.

Coale, K. H., et al., A massive phytoplankton bloom induced by an ecosystem-scale iron fertilization experiment in the equatorial Pacific Ocean, *Nature*, *383*, 495–501, 1996.

Craig, H., Abyssal carbon and radiocarbon in the Pacific, *J. Geophys. Res.*, *74*(23), 5491–5506, 1969.

Crowley, T. J., Ice Age terrestrial carbon changes revisited, *Global Biogeochem. Cycles*, *9*(3), 377–390, 1995.

De La Rocha, C. L., M. A. Brzezinski, M. J. DeNiro, and A. Shemesh, Silicon-isotope composition of diatoms as an indicator of past oceanic change, *Nature*, *395*, 680–683, 1998.

Dickson, A. G., and C. Goyet, DOE Handbook of methods for the analysis of the various parameters of the carbon dioxide system in sea water; version 2, *ORNL/CDIAC-74*, Dep. of Energy, Washington, D. C., 1994.

Ditullio, G. R., and W. O. Smith, Relationship between dimethylsulfide and phytoplankton pigment concentrations in the Ross Sea, Antarctica, *Deep Sea Res., Part I*, *42*, 873–892, 1995.

Dugdale, R. C., A. G. Wischmeyer, F. P. Wilkerson, R. T. Barber, F. Chai, M. Jiang, and T.-H. Peng, Dependence of equatorial Pacific export production and pCO_2 on silica trapping in the Southern Ocean: Implications for paleo-oceanography and paleo-climatology, paper presented at Oceanography Society Biennial Scientific Meeting, Miami Beach, Fla., 2–5 April 2001.

Fairbanks, R. G., A 17,000-year glacio-eustatic sea level record: Influence of glacial melting rates on the Younger Dryas event and deep-ocean circulation, *Nature*, *342*, 637–642, 1989.

Farrell, J. W., and W. L. Prell, Climatic change and $CaCO_3$ preservation: An 800,000 year bathymetric reconstruction from the central equatorial Pacific Ocean, *Paleoceanography*, *4*, 447–466, 1989.

Franck, V. M., M. A. Brzezinski, K. H. Coale, and D. M. Nelson, Iron and silicic acid concentrations regulate Si uptake north and south of the Polar Frontal Zone in the Pacific sector of the Southern Ocean, *Deep Sea Res., Part II*, *47*, 3315–3338, 2000.

Francois, R., M. A. Altabet, E.-F. Yu, D. M. Sigman, M. Bacon, M. Frank, G. Bohrmann, G. Bareille, and L. D. Labeyrie, Contribution of Southern Ocean surface-water stratification to low atmospheric CO_2 concentrations during the last glacial period, *Nature*, *389*, 929–935, 1997.

Froelich, P. N., V. Blanc, R. A. Mortlock, S. N. Chillrud, W. Dunstan, A. Udomkit, and T. H. Peng, River fluxes of dissolved silica to the ocean were higher during glacials: Ge/Si in diatoms, rivers, and oceans, *Paleoceanography*, *7*(6), 739–767, 1992.

Gnanadesikan, A., R. D. Slater, N. Gruber, and J. L. Sarmiento, Oceanic vertical exchange and new production: A comparison between models and observations, *Deep Sea Res., Part II*, *49*, 363–401, 2002.

Gordon, A., and B. A. Huber, Southern Ocean winter mixed layer, *J. Geophys. Res.*, *95*(C7), 11,655–11,672, 1990.

Gruber, N., Anthropogenic CO_2 in the Atlantic Ocean, *Global Biogeochem. Cycles*, *12*(1), 165–192, 1998.

Guilderson, T., R. G. Fairbanks, and J. L. Rubenstone, Tropical temperature variations since 20,000 years ago: Modulating interhemispheric climate change, *Science*, *263*, 663–665, 1994.

Harrison, K. G., Role of increased marine silica input on paleo-pCO_2 levels, *Paleoceanography*, *15*(3), 292–298, 2000.

Hurd, D. C., and S. Birdwhitell, On producing a more general model for biogenic silica dissolution, *Am. J. Sci.*, *283*, 1–28, 1983.

Hutchins, D. A., and K. W. Bruland, Iron-limited diatom growth and Si:N uptake ratios in coastal upwelling regime, *Nature*, *393*, 561–564, 1998.

Ingle, S. E., C. H. Culberson, J. E. Hawley, and R. M. Pytkowicz, The solubility of calcite in seawater at atmospheric pressure and 35‰ salinity, *Mar. Chem.*, *1*, 295–307, 1973.

Kamatani, A., Dissolution rates of silica from diatoms decomposing at various temperatures, *Mar. Biol. Berlin*, *68*, 91–96, 1982.

Keir, R. S., The dissolution kinetics of biogenic calcium carbonates in seawater, *Geochim. Cosmochim. Acta*, *44*, 241–252, 1980.

Knox, F., and M. B. McElroy, Changes in atmospheric CO_2: Influence of the Maine biota at high latitudes, *J. Geophys. Res.*, *89*(D3), 4629–4637, 1984.

Kumar, N., R. F. Anderson, R. A. Mortlock, P. N. Froelich, P. Kubik, B. Dittrich-Hannen, and M. Suter, Increased biological productivity and export production in the glacial Southern Ocean, *Nature*, *378*, 675–680, 1995.

Laws, E. A., P. G. Falkowski, W. O. Smith Jr., H. Ducklow, and J. J.

McCarthy, Temperature effects on export production in the open ocean, *Global Biogeochem. Cycles*, *14*(4), 1231–1246, 2000.
Legrand, M., C. Feniet-Saigne, E. S. Saltzman, G. Germain, N. I. Barkoc, and V. N. Petrov, Ice-core record of oceanic emissions of dimethylsulphide during the last climate cycle, *Nature*, *350*, 144–146, 1991.
Leuenberger, M., U. Siegenthaler, and C. C. Langway, Carbon isotope composition of atmospheric CO_2 during the last ice age from an Antarctic ice core, *Nature*, *357*, 488–490, 1992.
Levitus, S., and T. P. Boyer, *World Ocean Atlas* 1994, vol. 4, *Temperature*, Natl. Oceanic and Atmos. Admin., Washington, D. C., 1994.
Levitus, S., M. E. Conkright, J. L. Reid, R. G. Najjar, and A. Mantyla, Distribution of nitrate, phosphate and silicate in the world oceans, *Progr. Oceanogr.*, *31*, 245–273, 1993.
Levitus, S., R. Burgett, and T. P. Boyer, *World Ocean Atlas 1994*, vol. 3, *Salinity*, Natl. Oceanic and Atmos. Admin., Washington, D. C., 1994.
Li, Y.-H., T. Takahashi, and W. S. Broecker, Degree of saturation of $CaCO_3$ in the oceans, *J. Geophys. Res.*, *74*(23), 5507–5525, 1969.
Lynch-Stieglitz, J., T. F. Stocker, W. S. Broecker, and R. G. Fairbanks, The influence of air-sea exchange on the isotopic composition of oceanic carbon: Observations and modeling, *Global Biogeochem. Cycles*, *9*(4), 653–665, 1995.
Maier-Reimer, E., Geochemical cycles in an ocean general circulation model: Preindustrial tracer distributions, *Global Biogeochem. Cycles*, *7*(3), 645–677, 1993.
Maier-Reimer, E., and R. Bacastow, Modeling of geochemical tracers in the ocean, in *Climate-Ocean Interaction*, edited by M. E. Schlesinger, pp. 233–267, Kluwer Acad., Norwell, Mass., 1990.
Martin, J. H., Iron as a limiting factor in oceanic productivity, in *Primary Productivity and Biogeochemical Cycles in the Sea*, edited by P. G. Falkowski and A. D. Woodhead, pp. 123–137, Plenum, New York, 1992.
Martin, J. H., and S. E. Fitzwater, Iron deficiency limits phytoplankton growth in the north-east Pacific subarctic, *Nature*, *331*, 341–343, 1988.
Martin, J. H., et al., Testing the iron hypothesis in ecosystems of the equatorial Pacific Ocean, *Nature*, *371*, 123–129, 1994.
Martin, W. R., and F. L. Sayles, $CaCO_3$ dissolution in sediments of the Ceara Rise, western equatorial Atlantic, *Geochim. Cosmochim. Acta*, *60*, 243–263, 1996.
Matsumoto, K., J. Lynch-Stieglitz, and R. F. Anderson, Similar glacial and Holocene Southern Ocean hydrography, *Paleoceanography*, *16*(5), 445–454, 2001.
McCartney, M. S., Subantarctic mode water, *Deep Sea Res.*, *24*, Suppl., 103–119, 1977.
Millero, F. J., Thermodynamics of the carbon dioxide system in the oceans, *Geochim. Cosmochim. Acta*, *59*, 661–677, 1995.
Mook, W. G., J. C. Bommerson, and W. H. Straverman, Carbon isotope fraction between dissolved bicarbonate and gaseous carbon dioxide, *Earth Planet. Sci. Lett.*, *22*, 169–176, 1974.
Najjar, R. G., and J. C. Orr, Biotic how to, internal OCMIP report, 15 pp., Lab.des Sci. du Climat et l'Environ., Saclay, Gif-sur-Yvette, France, 1999.
Nelson, D. M., P. Tréguer, M. A. Brzezinski, A. Leynaert, and B. Quéguiner, Production and dissolution of biogenic silica in the ocean: Revised global estimates, comparison with regional data and relationship to biogenic sedimentation, *Global Biogeochem. Cycles*, *9*(3), 359–372, 1995.
Nelson, D. M., et al., Vertical budgets for organic carbon and biogenic silica in the Pacific Sector of the Southern Ocean, 1996–1998, *Deep Sea Res., Part II*, *49*, 1645–1673, 2002.
Orsi, A. H., T. I. Whitworth, and W. D. J. Nowlin, On the meridional extent and fronts of the Antarctic Circumpolar Current, *Deep Sea Res., Part I*, *42*, 631–673, 1995.
Petit, J. R., et al., Climate and atmospheric history of the past 420,000 years from Vostok ice core, Antarctica, *Nature*, *399*, 429–436, 1999.
Pondaven, P., D. Ruiz-Pino, C. Frabalo, P. Treguer, and C. Jeandel, Interannual variability of Si and N cycles at the time-series station KERFIX between 1990 and 1995: A 1-D modelling study, *Deep Sea Res., Part I*, *47*, 223–257, 2000.
Press, W. H., B. R. Flannery, S. A. Teukolsky, and W. T. Vetterling, *Numerical Recipes*, 818 pp., Cambridge Univ. Press, New York, 1992.
Rostek, F., G. Ruhland, F. C. Bassinot, P. J. Muller, L. Labeyrle, Y. Lancelot, and E. Bard, Alkenone paleotemperatures for the last 150,000 years for an equatorial Indian Ocean core, *Nature*, *364*, 319–321, 1993.
Sabine, C. L., R. M. Key, K. M. Johnson, F. J. Millero, A. Poisson, J. L. Sarmiento, D. W. R. Wallace, and C. D. Winn, Anthropogenic CO_2 inventory of the Indian Ocean, *Global Biogeochem. Cycles*, *13*(1), 179–198, 1999.
Sarmiento, J. L., and J. R. Toggweiler, A new model for the role of the oceans in determining atmospheric pCO_2, *Nature*, *308*, 621–624, 1984.
Shackleton, N. J., Carbon-13 in Uvigerina: Tropical rainforest history and the equatorial Pacific carbonate dissolution cycles, in *Fate of Fossil Fuel CO_2 in the Oceans*, edited by A. Malahoff, pp. 401–427, Plenum, New York, 1977.
Shackleton, N. J., The 100,000-year ice age cycle identified and found to lag temperature, carbon dioxide, and orbital eccentricity, *Nature*, *289*, 1897–1901, 2000.
Siegenthaler, U., and F. Joos, Use of a simple model for studying oceanic tracer distributions and the global carbon cycle, *Tellus, Ser. B*, *44*, 186–207, 1992.
Siegenthaler, U., and K. O. Munnich, $^{13}C/^{12}C$ Fractionation during CO_2 transfer from air to sea, in *Carbon Cycle Modelling*, edited by B. Bolin, pp. 249–257, John Wiley, New York, 1981.
Siegenthaler, U., and T. Wenk, Rapid atmospheric CO_2 variations and ocean circulation, *Nature*, *308*, 624–626, 1984.
Sigman, D. M., and E. A. Boyle, Glacial/interglacial variations in atmospheric carbon dioxide, *Nature*, *407*, 859–869, 2000.
Sigman, D. M., D. C. McCorkle, and W. R. Martin, The calcite lysocline as a constraint on glacial/interglacial low-latitude production changes, *Global Biogeochem. Cycles*, *12*(3), 409–427, 1998.
Smith, H. J., H. Fischer, M. Wahlen, D. Mastroianni, and B. Deck, Dual modes of the carbon cycle since the Last Glacial Maximum, *Nature*, *400*, 248–250, 1999.
Smith, W. O. J., R. F. Anderson, J. K. Moore, L. A. Codispoti, and J. M. Morrison, The US Southern Ocean Joint Global Ocean Flux Study: An introduction to AESOPS, *Deep Sea Res., Part II*, *47*, 3073–3093, 2000.
Stuiver, M., Workshop on ^{14}C data reporting, *Radiocarbon*, *22*(3), 964–966, 1980.
Stute, M., P. Schlosser, J. F. Clark, and W. S. Broecker, Paleotemperatures in the southwestern United States derived from noble gases in ground water, *Science*, *256*, 1000–1003, 1992.
Takeda, S., Influence of iron availability of nutrient consumption ratio of diatoms in oceanic waters, *Nature*, *393*, 774–777, 1998.
Toggweiler, J. R., Variation of atmospheric CO_2 by ventilation of the ocean's deepest water, *Paleoceanography*, *14*(5), 571–588, 1999.
Toggweiler, J. R., and J. L. Sarmiento, Glacial to interglacial changes in atmospheric carbon dioxide: The critical role of ocean surface water in high latitudes, in *The Carbon Cycle and Atmospheric CO_2: Natural Variations Archean to Present*, *Geophys. Monogr. Ser.*, vol. 32, edited by E. T. Sundquist and W. S. Broecker, pp. 163–184, AGU, Washington, D.C., 1985.
Toggweiler, J. R., K. Dixon, and K. Bryan, Simulations of radiocarbon in a coarse resolution world ocean model, 1, Steady-state prebomb distributions, *J. Geophys. Res.*, *94*(C6), 8217–8242, 1989.
Treguer, P., and P. Pondaven, Silica control of carbon dioxide, *Nature*, *406*, 358–359, 2000.
Vogel, J. G., P. M. Grootes, and W. G. Mook, Isotopic fractionation between gaseous and dissolved carbon dioxide, *Z. Phys.*, *230*, 225–238, 1970.
Weiss, R. F., W. S. Broecker, H. Craig, and D. Spencer, GEOSECS Indian Ocean Expedition, in *Hydrographic Data 1977–1978*, 48 pp., Natl. Sci. Found., Washington, D. C., 1983.
Yamanaka, Y., and E. Tajika, Role of dissolved organic matter in the marine biogeochemical cycle: Studies using an ocean biogeochemical general circulation model, *Global Biogeochem. Cycles*, *11*(4), 599–612, 1997.
Zhang, J., P. D. Quay, and D. O. Wilbur, Carbon isotope fractionation during gas-water exchange and dissolution of CO_2, *Geochim. Cosmochim. Acta*, *59*, 107–114, 1995.

M. Brzezinski, Department of Ecology and Evolution and Marine Biology and Marine Sciences Institute, University of California at Santa Barbara, Santa Barbara, CA 93106, USA. (brzezins@lifesci.ucsb.edu)

K. Matsumoto and J. Sarmiento, Program in Atmospheric and Oceanic Sciences, Princeton University, Princeton, NJ 08544, USA. (kmatsumo@splash.princeton.edu; jls@princeton.edu)